american physiological society

JNP JOURNAL OF NEUROPHYSIOLOGY

J Neurophysiol 134: 1359–1377, 2025.
First published September 24, 2025; doi:10.1152/jn.00331.2025

RESEARCH ARTICLE

Control of Movement

Speed-dependent locomotor adjustments following staggered thoracic lateral hemisections in adult cats

Sirine Yassine,[1]* Johannie Audet,[1]* Charly G. Lecomte,[1] Stephen Mari,[1] Angèle N. Merlet,[1] Jonathan Harnie,[1] Ilya A. Rybak,[2] Boris I. Prilutsky,[3] and Alain Frigon[1]

[1]*Department of Pharmacology-Physiology, Faculty of Medicine and Health Sciences, Centre de recherche du CHUS, Université de Sherbrooke, Sherbrooke, Quebec, Canada;* [2]*Department of Neurobiology and Anatomy, College of Medicine, Drexel University, Philadelphia, Pennsylvania, United States; and* [3]*School of Biological Sciences, Georgia Institute of Technology, Atlanta, Georgia, United States*

Abstract

Animals adjust their locomotor pattern to increased speed demands by decreasing stance/extensor phase duration while the swing/flexor phase remains relatively unchanged, which we refer to here as "stance/extensor dominance." The control of locomotor speed involves dynamic interactions between spinal circuits, supraspinal drive, and somatosensory feedback. Whereas complete spinal cord injuries abolish brain-spinal cord interactions, incomplete lesions, such as lateral hemisections, preserve some connectivity between brain and spinal circuits. In this study, we investigated adjustments in the locomotor pattern at different treadmill speeds before and after staggered lateral thoracic hemisections performed on opposite sides of the spinal cord (first at right T5–T6 and then at left T10–T11). We collected kinematic and electromyographic data during treadmill locomotion from 0.4 to 0.8 m/s before and 8 wk after each spinal lesion in eight adult cats. Our main results show left-right asymmetries in hindlimb phase durations after each lesion, with prolonged swing on the ipsilesional side and prolonged stance on the contralesional side across speeds. Hindlimb stance dominance was also weakened on the side of each lesion, first on the right and then on the left after the first and second hemisections, respectively. In contrast to phase durations, hindlimb stride lengths remained symmetrical after both injuries across speeds. Using our recent computational models and experimental data of the present study, we provide predictions of altered interactions between supraspinal drive and somatosensory feedback onto flexor and extensor half-centers to explain left-right changes in hindlimb phase durations across speeds after staggered lateral thoracic hemisections.

NEW & NOTEWORTHY Staggered lateral thoracic hemisections reversibly altered the temporal structure of the hindlimb locomotor cycle by reducing stance/extensor phase dominance in the ipsilesional hindlimb in favor of the swing/flexor phase. The contralateral hindlimb compensated by prolonging stance and reducing swing. The forelimbs started taking more steps within a hindlimb cycle independently of speed or lesion side. These results can be explained by reorganized sensorimotor interactions based on network architecture from recently published computational models.

lateral thoracic hemisection; locomotion; sensorimotor interactions; speed

INTRODUCTION

Animals, including humans, continuously adjust their locomotor speed to meet environmental and behavioral demands. This requires precise limb and trunk movements, controlled by dynamic interactions between central and peripheral neural mechanisms (1–3). Spinal cord injury (SCI) disrupts descending motor and ascending somatosensory pathways, altering dynamic sensorimotor interactions between different parts of the nervous system, including those involved in controlling locomotion and modulating speed. People with SCI walk much more slowly (4–8). However, animals, such as cats,

*S. Yassine and J. Audet contributed equally to this work.
Correspondence: A. Frigon (alain.frigon@usherbrooke.ca).
Submitted 1 July 2025 / Revised 23 July 2025 / Accepted 18 September 2025

maintain the ability to adjust their pattern to different speeds on a treadmill after a complete thoracic SCI (9–13). This is because proprioceptive and tactile inputs can still access and inform the spinal locomotor network below the SCI, directing it to change its output to adjust to treadmill speed. Humans with a clinically complete SCI can also step on a treadmill with electrical epidural stimulation of the spinal cord (14), but the effects of different treadmill speeds have not been specifically tested. Less is known about the control of locomotor speed after incomplete SCI, where spared supraspinal pathways can still interact with spinal sensorimotor circuits (15–17). For instance, after a lateral thoracic hemisection, cats recover quadrupedal treadmill locomotion up to speeds of 0.8–1.0 m/s (16–18), but notable left-right asymmetries appear in stance and swing phase durations (17), muscle activity (16), and hindlimb kinematics (15).

To explain how spinal sensorimotor circuits control locomotor cycle and phase durations with a change in speed before and after SCI, we recently developed computational models of hindlimb locomotion based on experimental data obtained in intact cats as well as after complete (i.e., spinal cats) or incomplete (lateral hemisection) lesions of the thoracic spinal cord (3, 19). We showed that spinal locomotor networks operate in a state machine regime at low speeds in intact cats and at all speeds in spinal cats. A state machine is a behavior that operates in only one of a finite number of states at any given time. It may change its state (e.g., a phase transition) only in response to an external input (20, 21). In the spinal-transected model, phase transitions were entirely dependent on somatosensory feedback from the hindlimbs. In the intact model, at higher speeds, the operation of the spinal locomotor network switches to a flexor-driven regime and then to a classical half-center regime, relying more on supraspinal drive. Our hemisected model proposed that the lesioned side is primarily controlled by somatosensory feedback, while the contralesional side is controlled by supraspinal drive. In the hemisected model, we considered the lesioned side as "transected" (i.e., completely cut off from descending commands) and the contralesional side as "intact" (i.e., receiving full supraspinal inputs).

However, what happens to the control of cycle and phase durations as a function of speed if a second contralateral hemisection is performed a few spinal segments below the first one? How does the system compensate for the bilateral loss of direct supraspinal drive with these staggered hemisections? Does the second hemisection generate a state resembling a complete transection, or do residual descending inputs continue to influence locomotor control and speed modulation? Does the second lateral hemisection mitigate, counteract, or neutralize left-right temporal or spatial asymmetries induced by the first hemisection with a change in speed? Unlike a single unilateral hemisection or complete spinal transection, staggered thoracic hemisections create a unique disruption of ascending and descending pathways (22–25). Previous studies using this paradigm have shown that the second hemisection can reverse left-right asymmetries in hindlimb stance and swing durations observed after the first hemisection, but this was only tested at a single treadmill speed of 0.4 m/s (26). It remains unclear how speed variations influence these asymmetries.

Therefore, the purpose of this study was to assess kinematic and electromyographic (EMG) changes in the locomotor pattern at different treadmill speeds following staggered lateral thoracic hemisections and use these data to uncover potential underlying mechanisms to explain changes. Specifically, we are interested in two types of somatosensory feedback that regulate the stance-to-swing transition, stretch-related feedback from hip flexors (27), which we can estimate by measuring hip angle, and hindlimb loading (28), which we can estimate by measuring extensor muscle activity. Our results show different adjustments in the locomotor pattern of the hindlimbs as a function of treadmill speed depending on the side of the lesions, with left-right phase duration asymmetries after the first hemisection that reversed after the second hemisection. Our experimental data provide additional mechanistic insight for our recent computational models (3, 19), testing the network architecture and sensorimotor interactions that we proposed to explain speed-dependent adjustments in the control of phase and cycle durations before and after SCI.

MATERIALS AND METHODS

Animals and Ethical Information

In accordance with policies and directives of the Canadian Council on Animal Care (Protocol no. 2022-3349), all procedures were approved by the Animal Care Committee of the Université de Sherbrooke. We collected the present dataset from eight adult cats, four females and four males, with mass between 4.1 and 6.5 kg (5.3 ± 1.0 kg). All animals completed the study, and no data were excluded. To reduce the number of animals used in research, all cats participated in other studies to investigate different scientific questions, some of which have been published (24–26, 29–32).

General Surgical Procedures

We performed all surgical procedures in an operating room, in aseptic conditions with sterilized equipment. Before surgery, cats were sedated with an intramuscular injection of butorphanol (0.4 mg/kg), acepromazine (0.1 mg/kg), and glycopyrrolate (0.01 mg/kg). We also administered ketamine-diazepam (0.05 mL/kg) intramuscularly for induction. We shaved the fur overlying the animals' back, stomach, and limbs with electric clippers and then cleaned the skin with chlorhexidine soap. Before intubation with a flexible endotracheal tube, we anesthetized the cats, using a mask with isoflurane (1.5–3%) delivered in O_2. We maintained anesthesia throughout the surgery, adjusting the level of isoflurane by assessing cardiac and respiratory rates, pupil size and reactivity, limb withdrawal reflexes, and jaw tone. We monitored body temperature with a rectal thermometer and maintained it within the physiological range (37–38°C) by adjusting the heat provided by an infrared lamp positioned ~50 cm above the animal and a water-filled heating pad placed underneath.

During surgery and for 7 h afterward, we injected a fast-acting analgesic (buprenorphine, 0.01 mg/kg) subcutaneously. We also administered a subcutaneous antibiotic (cefovecin, 0.1 mL/kg) and applied a transdermal fentanyl patch (25 μg/h) to the back of the animal, 2–3 cm rostral to the base

of the tail, providing prolonged analgesia for 4–5 days. After surgery, we closely monitored the cats in an incubator until they regained consciousness. At the end of the experiments, we euthanized the animals by administering a lethal dose of pentobarbital (120 mg/kg) through the left or right cephalic vein.

Electrode Implantation

To chronically record electromyography (EMG) from different limb muscles, we implanted pairs of Teflon-insulated multistrand fine wires (AS633; Cooner Wire Co., Chatsworth, CA). We directed these wires subcutaneously from two head-mounted 34-pin connectors (Omnetics Connector, Minneapolis, MN) to selected fore- and hindlimb muscles. For bipolar recordings, we stripped 1–2 mm of insulation from the wires and threaded them in the muscle belly with 23 gauge × 1½ in. needles, maintaining an ∼1-cm interelectrode distance between wires. Then, we verified the placement of each electrode by electrically stimulating the corresponding muscle through the appropriate head connector channel. Finally, we secured the head connector to the skull with six metallic screws and dental acrylic.

Staggered Lateral Hemisections

After collecting data in the intact state, we performed a first lateral hemisection on the right side of the spinal cord between the fifth and sixth thoracic vertebrae (T5–T6), following the same general surgical procedures described above. During surgery, we incised the skin covering the area of interest and carefully set aside the muscles and connective tissues. We then performed a small dorsal laminectomy to expose the spinal cord. After exposing the spinal cord, we applied lidocaine hydrochloride (2%) topically as an anesthetic and made two or three injections within the targeted region. Using surgical scissors, we hemisected the right side starting from the midline and proceeded laterally. We then stopped any residual bleeding. Before closing the incision, we placed a hemostatic material (Spongostan Dental; Ethicon Inc., Somerville, NJ) within the lesion site.

We collected data for 8–12 wk after the first hemisection up to when cats reached a visible plateau in locomotor recovery. We then performed a second lateral hemisection on the left side of the spinal cord between the 10th and 11th thoracic vertebrae (T10–T11). Surgical procedures and postsurgical care were the same for both injuries. After surgeries, we monitored the cats for voluntary bodily functions. Experienced personnel manually expressed their bladders and large intestines as needed, and we frequently cleaned the lower half of the animals to prevent infections. Data collection lasted for 8–12 wk after the second hemisection.

Experimental Protocol

Before electrode implantation, we trained all cats to walk on a treadmill at speeds up to 1.0 m/s. The treadmill consisted of two independently controlled running surfaces, each 120 cm long and 30 cm wide (Bertec, Columbus, OH). The two belts were separated by a Plexiglas separator (10 cm high and 1.0 cm wide; Avrex Canada Inc., Boucherville, QC, Canada) placed between the limbs to prevent them from impeding each other. For this study, we collected kinematic and EMG data at three different time points: the intact state and 7–8 wk after each hemisection, at speeds ranging from 0.4 to 0.8 m/s with 0.1 m/s speed increments because some cats could not step up to 1.0 m/s after the first (HO, KA, PO, TO) and/or second (AR, HO, JA, KA, PO, TO) hemisection. During each trial, we collected a sequence of at least 10 consecutive cycles. We used positive reinforcement (e.g., food, affection) and gave cats at least 30-s rest periods between trials to avoid fatigue.

After hemisections, we did not specifically train cats to recover quadrupedal locomotion. However, we collected data in other tasks on the treadmill, such as split-belt locomotion (with left and right limbs stepping at different speeds) and on a custom-made walkway (30, 32). We also evoked cutaneous reflexes in some cats at different speeds during tied- and split-belt locomotion (24, 25). These tasks can be considered a form of training. After hemisections, some cats required mediolateral balance assistance that we provided by slightly holding their tail without providing weight support (see Table 1 of Ref. 26). We applied perineal stimulation as needed to increase spinal excitability and facilitate hindlimb locomotion (33). To ensure consistency, the same experimenter manually pinched or rubbed the skin of the perineal region during stimulation. This approach prevented bias, as overly strong perineal stimulation can generate exaggerated flexion of the hindlimbs or impair left-right alternation. The strength of the stimulation was adjusted on a case-by-case basis to achieve optimal locomotor patterns.

Data Acquisition and Analysis

Data acquisition.

We recorded videos from the left and right sides with two cameras (Basler AcA640-100g; Basler, Ahrensburg, Germany) operating at 60 frames/s with a resolution of 640 × 480 pixels. We acquired EMG signals that were preamplified (10×, custom-made system), band-pass filtered (30–1,000 Hz), and amplified (100–5,000×), using a 16-channel amplifier (A-M Systems model 3500, Sequim, WA). We digitized the signals (5,000 Hz) with a National Instruments card (NI 6032E) and acquired them with custom software before storing them on a computer. We synchronized the recorded images and EMG data, using a custom program developed in LabVIEW (RRID: IMSCR_014325). Because the data acquisition system was limited to 16 channels and we recorded from >16 muscles, we collected data twice at each speed, once for each connector.

Temporal analysis.

We analyzed videos offline, using a custom-made program to identify contacts and liftoffs for each limb. We defined paw contact as the first frame showing visible contact with the treadmill surface and liftoff as the frame showing the most caudal displacement of the toe. Using this information, we measured cycle, stance, and swing durations. Cycle duration represents the time interval between successive paw contacts of the same limb, whereas stance duration corresponds to the time between paw contact and liftoff. To measure swing duration, we subtracted stance duration from cycle duration. We averaged the temporal values for each limb. We also plotted stance and swing durations against

cycle durations to establish phase/cycle duration relationships. After the first or second hemisection, some cats displayed cycles where the forelimbs performed two cycles within one hindlimb cycle, or a 2:1 fore-hind pattern, as reported previously (15, 25, 33). These 2:1 patterns were often intermingled with 1:1 fore-hind patterns. The occurrence of 2:1 fore-hind patterns was quantified for each cat by calculating the number of cycles with two cycles of the same forelimb within one right hindlimb cycle, divided by the total number of cycles within a locomotor episode.

To determine whether the left-right locomotor pattern becomes asymmetrical after hemisection, we calculated an asymmetry index (AI) for individual cycle, stance, and swing durations by subtracting the left temporal value from the right one. The difference was normalized to the sum of both right and left variables, and the average AI was then computed over 10–20 consecutive locomotor cycles (17).

$$\mathrm{AI} = \frac{\text{Right value} - \text{Left value}}{\text{Right value} + \text{Left value}}$$

The sign of the AI value indicates the direction of the asymmetry, with zero indicating perfect right/left symmetry, negative values reflecting longer durations on the left compared to the right side, and positive values indicating longer durations on the right compared to the left side. We finally determined individual support periods based on contacts and liftoffs to measure when two, three, or four limbs were in contact with the treadmill and expressed them as a percentage of cycle duration (26, 30, 34). Within a normalized cycle, defined from successive right hindlimb contacts, we identified nine periods of limb support (26, 30, 34, 35).

Spatial analysis.

To analyze spatial variables, we used DeepLabCut (RRID: SCR_021391), an open-source machine learning tool powered by deep neural networks (36). We measured stride length as the distance between contact and liftoff of a limb, added to the distance traveled by the treadmill during the swing phase (26, 30, 37, 38). We also calculated an AI for stride lengths across all speeds before and after each hemisection. We also measured hip angles at liftoffs, defined as the angle at the greater trochanter between the iliac crest and the tibial head, across all speeds in the intact state and after each hemisection.

EMG analysis.

Although we implanted electrodes in several muscles, we focused our analysis on six muscles of the right (R) and left (L) limbs: the biceps brachii (BB), an elbow flexor and shoulder protractor (LBB, $n = 5$; RBB, $n = 5$); the extensor carpi ulnaris (ECU), a wrist dorsiflexor (LECU, $n = 5$; RECU, $n = 6$); the long head of triceps brachii (TRI), an elbow extensor and shoulder retractor (LTRI, $n = 6$; RTRI, $n = 7$); the lateral gastrocnemius (LG), an ankle plantarflexor and knee flexor (LLG, $n = 5$; RLG, $n = 5$); the soleus (SOL), an ankle plantarflexor (LSOL, $n = 5$; RSOL, $n = 4$); and the anterior sartorius (SRT), a hip flexor and knee extensor (LSRT, $n = 6$; RSRT, $n = 5$). We used a custom program to calculate burst durations and mean amplitudes after visually identifying burst onsets and offsets. Burst duration was measured from onset to offset, and mean amplitude was calculated by integrating the full-wave rectified burst from onset to offset and dividing it by its duration. We expressed EMG burst amplitudes as percentages of the maximal value obtained across the five speeds and three spinal states (intact, Hemi1, and Hemi2) within each muscle and animal to provide a normalized EMG amplitude.

Histology

To confirm the extent of the lesions, we collected spinal cord sections for histological analysis. After euthanizing the cats, we removed a 2-cm-long spinal segment at each lesion. We fixed the segment in 25 mL of 4% paraformaldehyde prepared in 0.1 M phosphate-buffered saline (PBS) and stored it at 4°C. After 5 days, we cryopreserved the segments in a 30% sucrose-PBS solution for 72 h at 4°C. Then, we sliced the spinal cord into 50-μm coronal sections with a cryostat (CM1860; Leica BioSystems Inc., Concord, ON, Canada) and mounted the sections on gelatinized slides. After drying the slides overnight, we stained them with 1% cresyl violet for 12 min, washed them in water for 3 min, and dehydrated them in successive ethanol baths for 5 min (50%, 70%, 100%). Finally, we cleared the slides in xylene, mounted them with dibutyl phthalate polystyrene xylene (Sigma-Aldrich Canada), and scanned them with a Nanozoomer 2.0-RS (Hamamatsu Corp., Bridgewater, NJ). Using ImageJ (RRID:SCR_003070), we reconstructed the lesion of the slide with the most identifiable damage. We estimated the lesioned area by dividing the area of the scarring tissue stained with cresyl violet acetate by the total area of the selected slice and expressed it as a percentage (24–26, 30, 32).

Statistical Analysis

We used a linear mixed-effects model to assess the effects of speed and spinal state on all outcome variables, including the occurrence of 2:1 patterns, cycle and phase durations, swing proportion, asymmetry indices, support periods, stride lengths, hip angles, and EMG variables. We performed the analysis with the lmer() function from the lme4 package in R software (version 2024.09.1; RRID:SCR_001905). The model included two fixed factors, State (levels: intact, Hemi1, Hemi2) and Speed (levels: 0.4, 0.5, 0.6, 0.7, and 0.8 m/s), as well as their interaction (State × Speed). To account for inter-individual variability and repeated measures, we included a random intercept (capturing baseline differences between cats) and a random slope (capturing variability in the effect of state across cats). We structured the model as follows: Variable ~ State × Speed + (1 + State|Cat_ID). We conducted a type III analysis of variance (ANOVA), using the car package to evaluate the main effects of State, Speed, and their interaction. This approach is equivalent to a two-way repeated-measures ANOVA but provides greater flexibility by accommodating interindividual variability and unbalanced data. For post hoc comparisons, we used the estimated model coefficients to assess differences between individual levels of State and Speed relative to their respective reference conditions (intact state and 0.4 m/s). No correction for multiple comparisons was applied.

We also calculated regression equations for stance/swing and cycle duration relationships with SigmaPlot (version

11.0; Systat Software; RRID:SCR_003210). For each phase and time point, we determined the slopes, the coefficient of determination (R^2), and Pearson's correlation coefficient (r). Then, we examined the relationship between phases and cycle duration and analyzed the effect of state on the slope of the phase-cycle duration relationship, using a one-factor repeated-measures ANOVA in IBM SPSS Statistics 26.0 (IBM Corp., Armonk, NY; RRID:SCR_002865). Finally, we performed a multiple regression analysis to determine whether the slope of phase and cycle durations differs between the stance and swing phases at each time point. We set the level of statistical significance at $P < 0.05$ for all tests.

RESULTS

Staggered Hemisections Affect Quadrupedal Locomotion and Coordination between the Fore- and Hindlimbs at Different Speeds

Based on histological analysis, we estimated the extent of the first (Fig. 1*A*) and second (Fig. 1*B*) spinal lesions for each cat. The first lesion (Hemi1) ranged from 40.3% to 66.4%, with a mean of 50.1 ± 9.1%, and the second (Hemi2) ranged from 33.5% to 53.7%, with a mean of 45.8 ± 6.5%. At 7–8 wk for Hemi1 and Hemi2, all eight cats could step on the treadmill over a range of speeds. Four of eight cats stepped up to 1.0 m/s after Hemi1 (AR, GR, JA, MB), but only two of these reached this speed after Hemi2 (GR, MB). Although all cats could walk from 0.4 m/s to 0.8 m/s at both time points post hemisection, all required mediolateral balance assistance at Hemi2 for all tested speeds. At Hemi1, all cats performed quadrupedal locomotion without perineal stimulation. At Hemi2, three of eight cats required perineal stimulation at all tested speeds (AR, MB, PO).

Figure 2 illustrates adjustments in the locomotor pattern to treadmill speed by showing EMG and stance phases at 0.4 and 0.8 m/s in one cat before and after staggered hemisections. In the intact state, this cat performed an equal number of forelimb and hindlimb locomotor cycles, or a 1:1 forelimb-hindlimb pattern (Fig. 2*A*). At 0.8 m/s, the stance phases and TRI/ECU/LG/SOL burst durations were visibly shorter compared to 0.4 m/s. At Hemi1 (Fig. 2*B*) and Hemi2 (Fig. 2*C*), this cat displayed 2:1 forelimb-hindlimb patterns, where a forelimb performed two cycles within one right hindlimb cycle. At Hemi1, the right hindlimb showed a prolonged swing phase and RSRT burst duration, which became shorter at 0.8 m/s. In contrast, the left hindlimb displayed a longer stance phase and LLG/LSOL burst durations, which also shortened at 0.8 m/s. At Hemi2, the left hindlimb showed a longer swing phase and LSRT burst duration, whereas its stance phase and LLG/LSOL burst durations were shortened compared to Hemi1. Meanwhile, the stance phase and RLG/RSOL burst durations became longer in the right hindlimb, whereas the swing phase and RSRT burst durations became shorter. At 0.8 m/s, these left-right differences persisted, with shorter stance/swing and LLG/LSOL/LSRT burst durations in the left hindlimb, whereas the right hindlimb only showed shorter stance and RLG/RSOL burst durations. Forelimb cycle, phase, and EMG burst durations slightly decreased with each hemisection as 2:1 fore-hind patterns emerged.

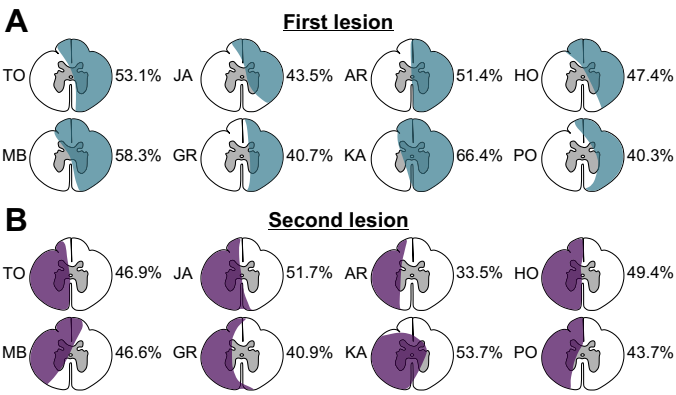

Figure 1. Extent of spinal lesions. Estimated extent of the first (*A*) and second (*B*) lesions performed at right (T5–T6) and left (T10–T11) thoracic levels, respectively, based on histological analysis of individual cats. The shaded areas indicate the lesioned regions. On the *left* and *right* of each diagram are the cat ID and lesion extent expressed as a percentage of total area, respectively.

For the group, at Hemi1 both the left and right forelimbs showed similar occurrence of 2:1 fore-hind patterns (Table 1). The occurrence of 2:1 patterns did not significantly change at Hemi2 compared to Hemi1 for LF ($P = 0.2$) and RF ($P = 0.1$). Similarly, the occurrence of 2:1 patterns was not significantly affected by treadmill speed for LF ($P = 0.7$) or RF ($P = 0.5$).

Staggered Hemisections Produce Limb- and Speed-Dependent Changes in Cycle and Phase Durations

Before and after hemisections, cycle duration significantly decreased with increasing speed in all four limbs for the group (Fig. 3*A*, significant main effect of speed). At Hemi1 and Hemi2, cycle duration was significantly shorter in the forelimbs (LF: Hemi1, $P < 0.001$; Hemi2, $P < 0.001$; RF: Hemi1, $P < 0.001$; Hemi2, $P < 0.001$) and longer in the hindlimbs (LH: Hemi1, $P = 0.008$; Hemi2, $P = 0.01$; RH: Hemi1, $P = 0.008$; Hemi2, $P = 0.009$) compared to the intact state (Fig. 3*A*, significant main effect of state). This is mainly due to the appearance of 2:1 fore-hind patterns. Before and after hemisections, stance duration significantly decreased with increasing speed in all four limbs (Fig. 3*B*, significant main effect of speed). At Hemi1 and Hemi2, stance duration was significantly shorter in LF (Hemi1, $P < 0.001$; Hemi2, $P < 0.001$) and RF (Hemi1, $P = 0.01$; Hemi2, $P < 0.001$) and longer at Hemi1 in LH ($P < 0.001$) before returning to intact values at Hemi2 (Fig. 3*B*, significant main effect of state). Stance duration did not significantly change in RH after hemisections. Before and after hemisections, speed significantly affected swing duration (Fig. 3*C*, significant main effect of speed). We mainly observed a slight decrease with increasing speed. We observed large changes in swing duration following hemisections, particularly in the hindlimbs (Fig. 3*C*, significant main effect of state). In LF (Hemi1, $P = 0.002$; Hemi2, $P < 0.001$) and RF (Hemi1, $P < 0.001$; Hemi2, $P < 0.001$), swing duration decreased at Hemi1 and Hemi2 compared to the intact state. At Hemi1 ($P < 0.001$) and Hemi2 ($P = 0.003$), swing duration was significantly longer in RH and at Hemi2 ($P = 0.003$) in LH compared to the intact state.

To assess left-right asymmetries in the hindlimbs across speeds after staggered hemisections, we measured an

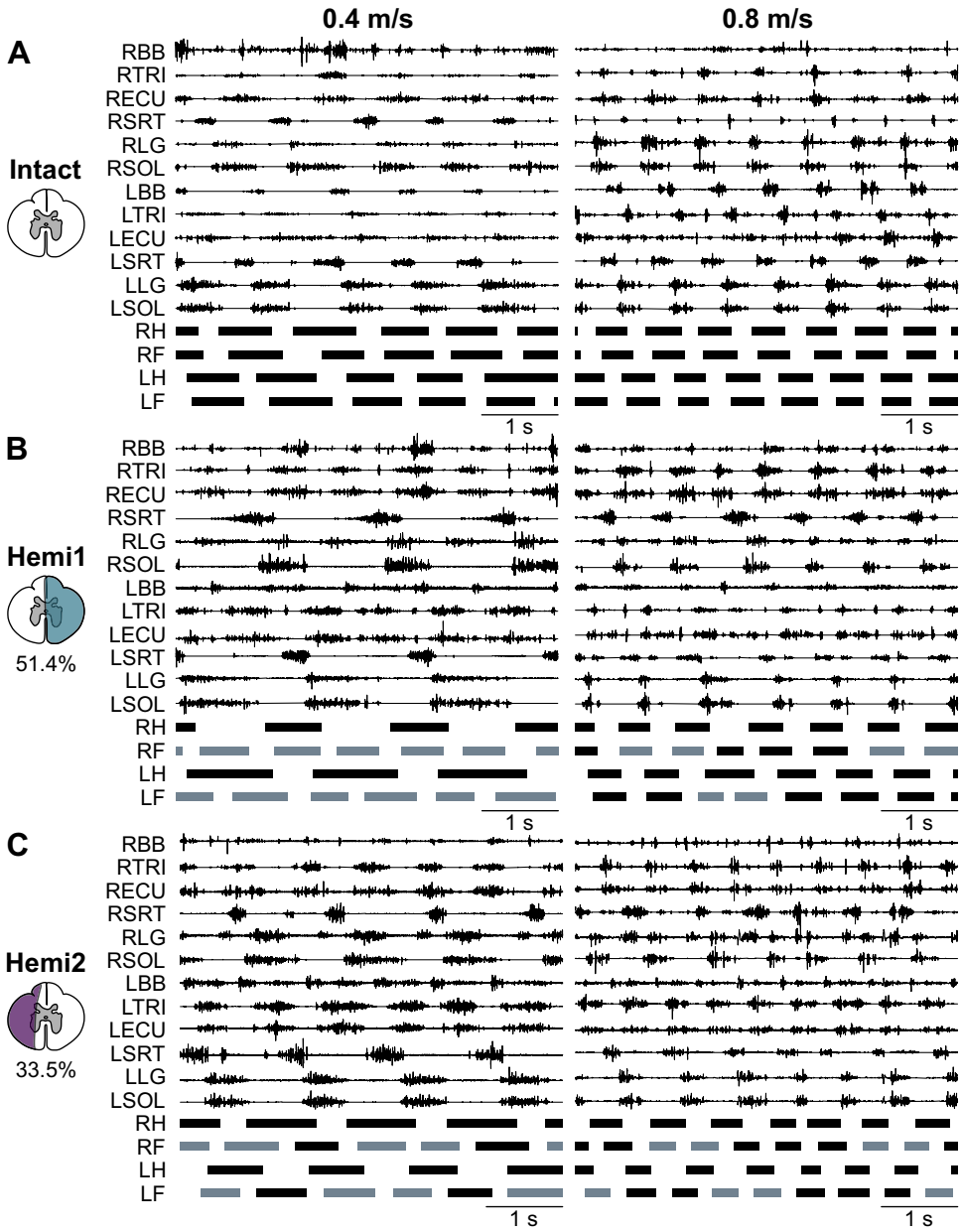

Figure 2. Locomotor adjustments to treadmill speed before and after staggered hemisections. Electromyography (EMG) waveforms and stance phases (thick horizontal lines) of the left and right limbs from a representative cat (AR) at 0.4 m/s and 0.8 m/s in the intact state (*A*) and 8 wk after first (Hemi1; *B*) and second (Hemi2; *C*) hemisections. Gray stance phases indicate cycles with 2:1 fore-hind patterns. The extent of each lesion is illustrated. BB, biceps brachii; ECU, extensor carpi ulnaris; F, forelimb stance; H, hindlimb stance; L, left; LG, lateral gastrocnemius; R, right; SOL, soleus; SRT, sartorius; TRI, triceps brachii.

asymmetry index (AI) (Fig. 4). The AI for cycle duration remained around 0 across speeds, indicating that both hindlimbs maintained a 1:1 pattern, or perfect left-right symmetry. On the other hand, stance and swing durations showed marked asymmetries after hemisections compared to the intact state. At Hemi1, left stance ($P < 0.001$) and right swing ($P < 0.001$) were significantly longer than right stance and left swing, respectively. At Hemi2, the pattern reversed with longer right stance and left swing, but despite a main effect of state, pairwise comparisons showed no significant differences compared to the intact state (stance, $P = 0.10$; swing, $P = 0.14$).

Table 1. *Occurrence of 2:1 fore-hind patterns after staggered hemisections*

	Hemi1		Hemi2	
Speed, m/s	LF	RF	LF	RF
0.4	35 ± 39%	35 ± 38%	51 ± 22%	51 ± 26%
0.5	41 ± 31%	42 ± 30%	52 ± 20%	48 ± 23%
0.6	39 ± 22%	40 ± 22%	47 ± 27%	49 ± 19%
0.7	41 ± 30%	41 ± 30%	56 ± 18%	50 ± 20%
0.8	32 ± 25%	34 ± 23%	48 ± 19%	48 ± 19%

Each value in the table is the mean ± SD percentage of 2:1 fore-hind patterns across treadmill speeds for the group ($n = 8$) after the first (Hemi1) and second (Hemi2) hemisections for the left (LF) and right (RF) forelimbs.

Staggered Hemisections Affect the Temporal Structure of the Locomotor Cycle across Speeds

Studies have shown that a change in cycle duration with speed is accompanied by a concomitant change in stance duration while swing duration remains relatively unchanged in cats and humans (10, 12, 37, 39–44). In other words, stance (extensor phase) duration controls or dominates cycle duration (45). To determine whether staggered thoracic hemisections

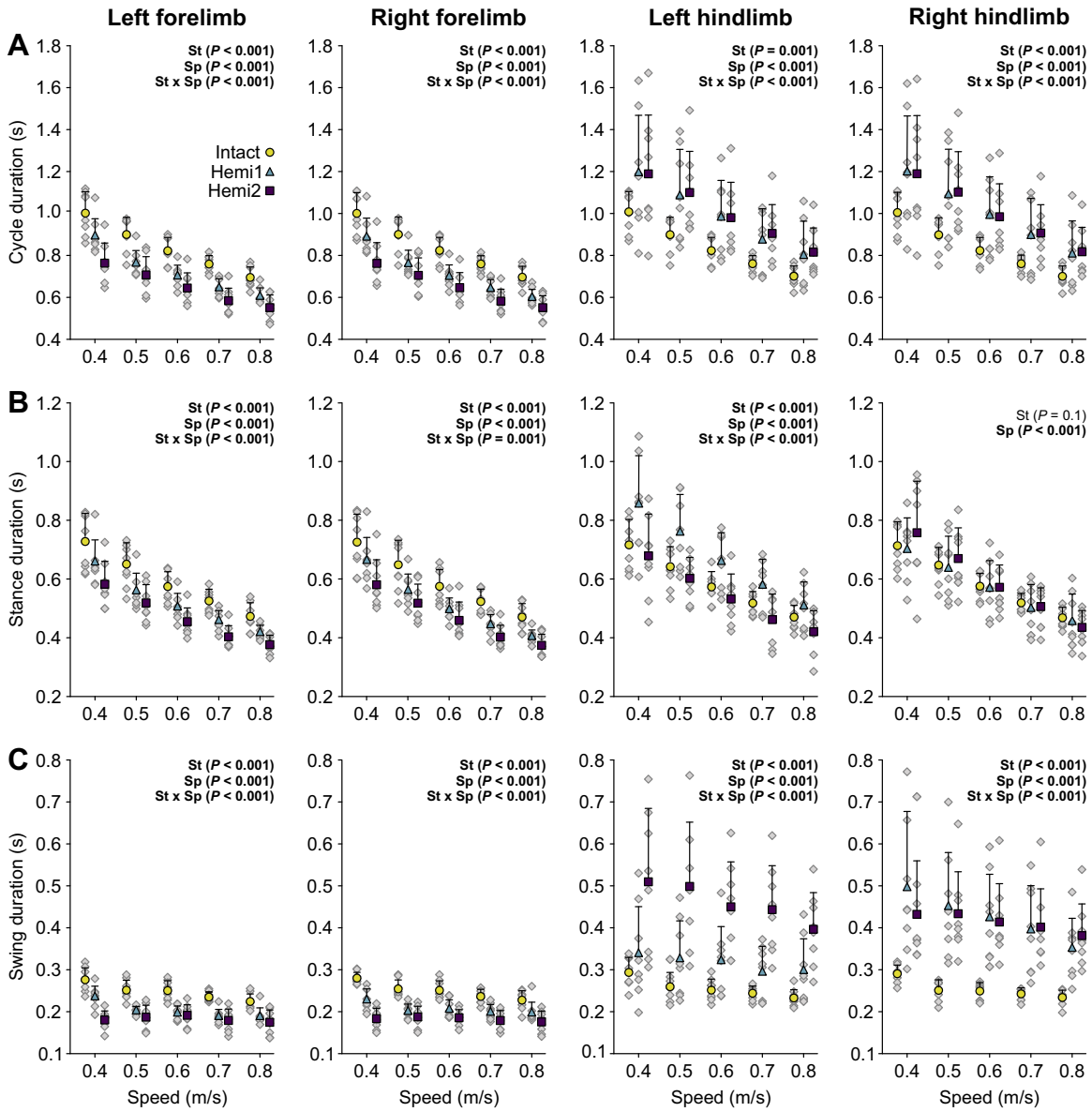

Figure 3. Temporal adjustments across speeds during quadrupedal treadmill locomotion before and after staggered hemisections. Cycle (*A*), stance (*B*), and swing (*C*) durations for the fore- and hindlimbs across treadmill speeds before and after hemisections. Data are represented as mean ± SD for each limb ($n = 8$ cats). Light gray diamonds represent means for individual cats from 8–36 cycles. *P* values for the main effects of state (St), speed (Sp), and their interaction (St × Sp) were obtained from a linear mixed-effects model followed by a type III ANOVA and are shown atop each panel. *P* values in bold indicate a significant main effect at <0.05. Hemi1, first hemisection; Hemi2, second hemisection.

affect this dominance, we plotted stance and swing durations as a function of cycle duration (Fig. 5) (17, 34, 40, 46). We then measured the slope (a), coefficient of determination (R^2), and Pearson's correlation coefficient (r) for the linear regressions of stance-cycle and swing-cycle relationships.

Overall, in the forelimbs, staggered hemisections did not affect stance dominance (Fig. 5, *A* and *B*). The slopes were significantly greater for stance-cycle duration relationships than for swing-cycle duration relationships in all three states in both forelimbs. The slope of the stance-cycle relationship was significantly more pronounced at Hemi2 in LF compared to the intact state ($P = 0.002$). In the hindlimbs, however, we observed notable changes after hemisections. At Hemi1, although stance dominance remained in LH (Fig. 5*C*, *center*), in RH (Fig. 5*D*, *center*) the cycle varied with both stance and swing. In RH, the slopes of stance-cycle and swing-cycle duration relationships were significantly smaller ($P = 0.009$) and greater ($P = 0.02$), respectively, compared to the intact state. At Hemi2, we observed a reversal, with cycle duration varying with both stance and swing phases in LH (Fig. 5*C*, *right*). In LH, the slopes of stance-cycle and swing-cycle duration relationships were significantly smaller ($P = 0.03$) and greater ($P = 0.03$), respectively, compared to the intact state. In RH, we observed a return of stance dominance, albeit weakened compared to the intact state (Fig. 5*D*, *right*). Thus, staggered hemisections affect the control of the cycle by its subphases, with weakened stance dominance on the side of the lesion.

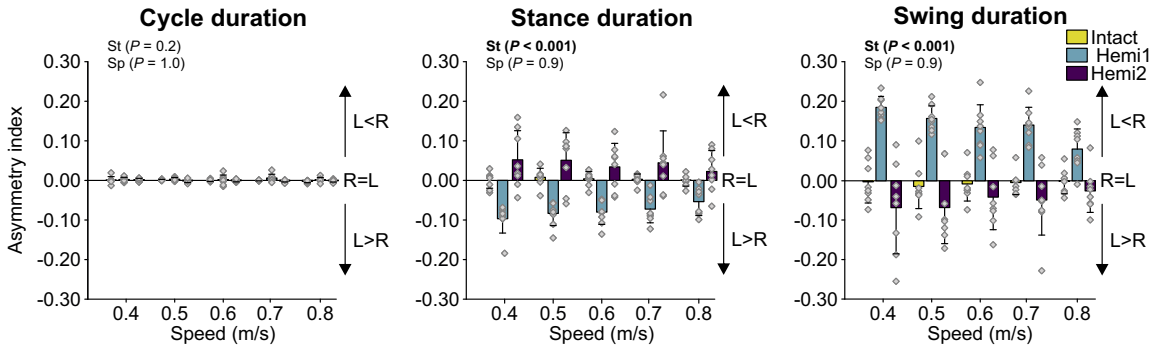

Figure 4. Asymmetry index of hindlimb cycle and phase durations at different speeds before and after staggered hemisections. The temporal asymmetry index was calculated between the right (R) and left (L) hindlimbs for cycle, stance, and swing durations across 5 locomotor speeds before and after lateral hemisections. Bars show mean ± SD ($n = 8$ cats), and light gray diamonds represent individual means. *P* values for the main effects of state (St), speed (Sp), and their interaction (St × Sp) were obtained from a linear mixed-effects model followed by a type III ANOVA and are shown atop each panel. *P* values in bold indicate a significant main effect at <0.05. Hemi1, first hemisection; Hemi2, second hemisection.

To determine why stance dominance changes after the first and second hemisections, we measured the proportion of swing as a function of the cycle, shown to positively correlate with weakened extensor/stance dominance and/or increased flexor/swing dominance (45–47). In both forelimbs, swing phase proportion significantly increased with increasing speed (Fig. 6*A*, significant main effects of speed). After hemisections, this proportion was significantly reduced in RF at Hemi1 ($P = 0.007$) and Hemi2 ($P < 0.001$), and in LF at Hemi2 ($P < 0.001$), compared to the intact state (Fig. 6*A*, significant main effects of state). However, these changes with speed were small. In both hindlimbs, we also observed a small but significant increase in swing proportion with speed (Fig. 6*B*, significant main effect of speed). Compared to the intact state, at Hemi1 swing proportion significantly increased in RH ($P < 0.001$) but not LH, whereas at Hemi2 swing proportion remained high in RH ($P = 0.003$) and considerably increased in LH ($P = 0.003$) (Fig. 6*B*, significant main effect of state).

Reorganization of Support Periods after Staggered Hemisections

To determine how animals adjust their limb coordination with a change in speed, we measured individual support periods before and after staggered hemisections. During quadrupedal locomotion, we identified nine individual support periods within a cycle, defined by the number of limbs contacting the treadmill at a given time (26, 29, 30, 34, 48). In the intact state, support *periods 1*, *3–5*, and *7–9* occupied the largest proportion of the cycle (Fig. 7, *left*, and Table 2). These are periods of triple and homolateral support. We rarely observed *periods 2* and *6*, diagonal support periods. *Periods 1*, *3*, *5*, *7*, and *9* decreased with increasing speed, whereas *periods 4* and *8*, right and left homolateral support periods, increased (Fig. 7, significant main effect of speed). All periods, except for *periods 4* and *9*, were significantly affected by state (Fig. 7, significant main effect of state). At Hemi1, *periods 1* ($P < 0.001$), *3* ($P = 0.04$), and *5* ($P = 0.005$) significantly decreased compared to the intact state while the diagonal support *period 6* ($P = 0.03$), involving RF and LH, significantly increased. Pairwise comparisons revealed no significant differences between Hemi1 and the intact state for support *periods 2*, *7*, and *8*. At Hemi2, *periods 1* ($P < 0.001$), *5* ($P < 0.001$), and *8* ($P = 0.03$) significantly decreased compared to the intact state while *periods 2* ($P < 0.001$), *3* ($P = 0.02$), *6* ($P < 0.001$), and *7* ($P = 0.02$) increased. Thus, staggered hemisection significantly increased diagonal support periods (*2* and *6*) and triple support periods involving both forelimbs (*3* and *7*) while decreasing triple support periods involving both hindlimbs (*1* and *5*).

Speed- and State-Dependent Modulation of Stride Length

Under normal conditions, increasing treadmill speed is associated with shorter cycle durations and longer stride lengths, enabling the limb to cover more distance in less time (34, 37, 49, 50). Here, we measured stride length values across speeds before and after staggered hemisections (Fig. 8). As expected, stride lengths significantly increased with increasing speed in both hindlimbs (Fig. 8*A*, significant main effect of speed). Compared to the intact state, stride lengths significantly increased for RH at Hemi1 ($P = 0.03$) and Hemi2 ($P = 0.01$) and at Hemi2 for LH ($P = 0.03$) (Fig. 8*A*, significant main effect of state). To quantify left-right asymmetries in stride lengths, we measured an AI before and after each hemisection (Fig. 8*B*). Interestingly, we observed no main effect of speed or state, indicating that stride lengths remain relatively symmetrical in the left and right hindlimbs, consistent with Audet et al. (26), which only looked at one speed.

Speed- and State-Dependent Modulation of Hip Angles at Liftoff

An important somatosensory signal regulating phase durations and transitions is related to hip angle and the length of hip flexors at the stance-to-swing transition (27, 51). Hip angle increased with increasing speed in both LH and RH (Fig. 9, significant main effects of speed). However, we found no significant main effect of state for LH. Although we observed a significant main effect of state for RH, pairwise comparisons revealed no significant differences between the intact state and Hemi1 ($P = 0.5$) or Hemi2 ($P = 0.3$). Thus, staggered hemisections did not affect hip angles at liftoff.

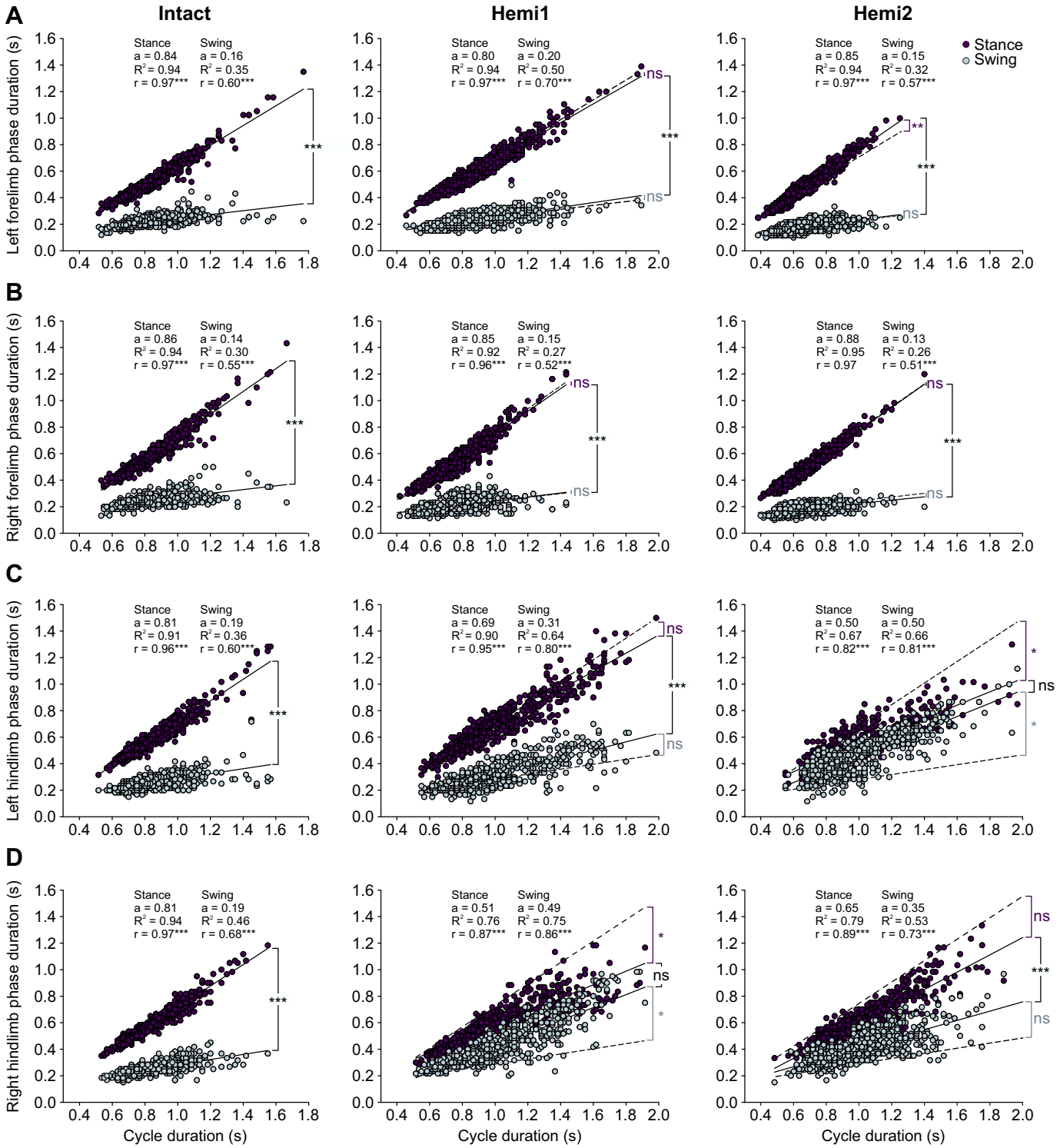

Figure 5. Phase-cycle duration relationships before and after staggered hemisections. *A* and *B*: forelimbs. *C* and *D*: hindlimbs. Stance (dark circles) and swing (blue circles) durations were plotted against cycle duration in the intact state (*left*), after the first hemisection (Hemi1, *center*), and after the second hemisection (Hemi2, *right*). Each circle represents a cycle, with ~8–15 cycles at each speed per cat ($n = 8$ cats). Dashed lines indicate the intact stance-cycle and swing-cycle slopes. $^{*}P < 0.05$; $^{**}P < 0.01$; $^{***}P < 0.001$; ns, nonsignificant. *a*, Slope; R^2, coefficient of determination; *r*, coefficient of correlation.

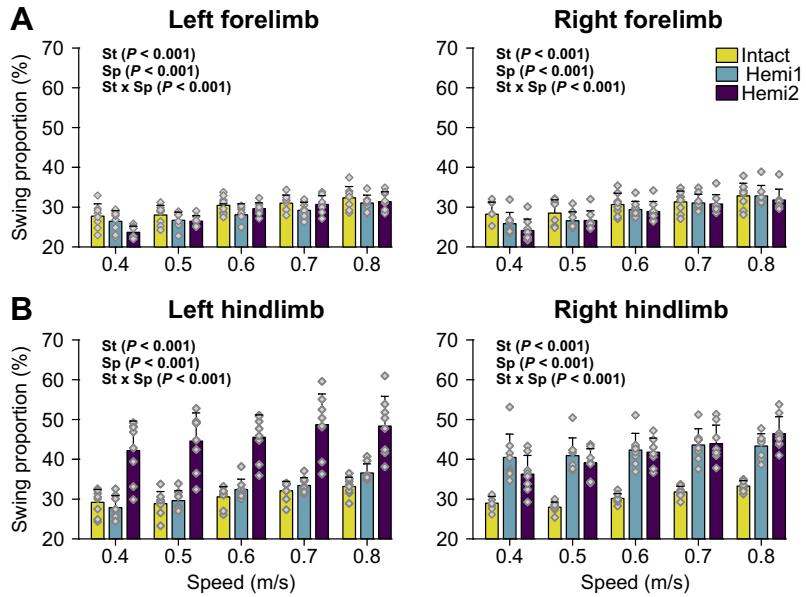

Figure 6. Swing proportion across speeds before and after staggered hemisections. Swing proportion was calculated for the forelimbs (*A*) and hindlimbs (*B*) across 5 locomotor speeds before and after lateral hemisections. Bars represent the mean ± SD ($n = 8$ cats), with light gray diamonds indicating individual means. *P* values for the main effects of state (St), speed (Sp), and their interaction (St × Sp) were obtained from a linear mixed-effects model followed by a type III ANOVA and are shown atop each panel. *P* values in bold indicate a significant main effect at <0.05. Hemi1, first hemisection; Hemi2, second hemisection.

Speed- and State-Dependent Modulation of Muscle Activity

To determine how staggered hemisections affected the neural drive to left and right limb muscles when changing speed, we measured EMG burst durations (Fig. 10) and amplitudes (Fig. 11) in selected muscles of the fore- and hindlimbs.

In the intact state, EMG burst durations significantly decreased with increasing speed in all forelimb and hindlimb muscles (Fig. 10, significant main effect of speed). At Hemi1, EMG burst duration significantly decreased for LBB ($P = 0.03$) and RLG ($P < 0.001$) but increased for LLG ($P = 0.04$), LSOL ($P < 0.001$), and RSRT ($P = 0.01$) compared to the intact state (Fig. 10, significant main effect of state). These changes shifted toward intact values at Hemi2. LSRT burst duration remained unchanged at Hemi1 but was significantly longer at Hemi2 ($P = 0.01$), and RBB burst duration was shorter at Hemi1 ($P = 0.006$) and Hemi2 ($P < 0.001$) compared to the intact state. The burst duration did not change for LTRI, RTRI, LECU, RECU, and RSOL after either hemisection.

In the intact state, the normalized EMG amplitude significantly increased with increasing speed for BB, TRI, ECU, SOL, LG, and SRT (Fig. 11, significant main effect of speed).

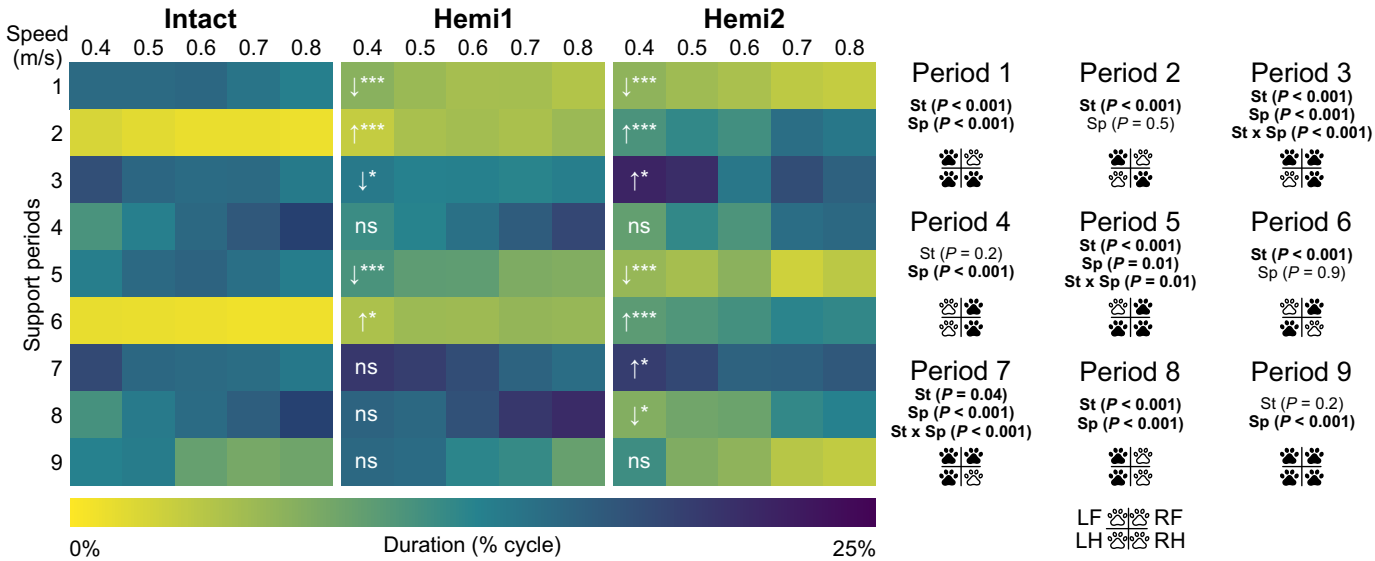

Figure 7. Support periods across speeds before and after staggered hemisections. The color maps on the *left* show 9 individual support periods, expressed as a percentage of right hindlimb cycle duration, at different speeds in the intact state (*left*), after the first hemisection (Hemi1, *center*), and after the second hemisection (Hemi2, *right*). Downward and upward arrows at Hemi1 and Hemi2 indicate a significant decrease and increase, respectively in support periods for all speeds compared to the intact state. In the diagrams on the *right*, black filled paws represent limbs in contact with the treadmill surface, and open/white paws indicate limbs in an aerial phase. *P* values for the main effects of state (St), speed (Sp), and their interaction (St × Sp) were obtained from a linear mixed-effects model followed by a type III ANOVA. *P* values in bold indicate a significant main effect at <0.05. LF, left forelimb; LH, left hindlimb; RF, right forelimb; RH, right hindlimb; *P* values of pairwise comparisons: *<0.05; ***<0.001; ns, nonsignificant.

Table 2. *Percentage of support periods across speeds and states*

State	Intact					Hemi1					Hemi2				
Speed, m/s	0.4	0.5	0.6	0.7	0.8	0.4	0.5	0.6	0.7	0.8	0.4	0.5	0.6	0.7	0.8
SP1	14.8 ± 2.3	14.9 ± 3.3	15.1 ± 2.7	13.8 ± 3.6	12.8 ± 3.1	6.7 ± 1.3	5.8 ± 1.1	5.1 ± 1.8	5.1 ± 1.7	4.3 ± 1.3	6.4 ± 2.8	5.5 ± 2.8	4.8 ± 4.8	3.7 ± 2.8	3.3 ± 2.1
SP2	2.2 ± 2.0	1.6 ± 2.9	1.1 ± 2.5	1.1 ± 1.6	0.9 ± 1.3	3.3 ± 2.4	4.9 ± 2.2	5.2 ± 2.9	4.8 ± 3.5	5.7 ± 3.2	10.4 ± 4.4	11.8 ± 3.0	10.9 ± 6.9	14.4 ± 4.5	13.5 ± 2.0
SP3	17.4 ± 4.9	15.2 ± 3.6	14.8 ± 3.9	14.8 ± 3.6	13.3 ± 3.8	13.4 ± 2.2	12.6 ± 2.5	12.7 ± 2.0	12.3 ± 2.2	12.8 ± 2.4	21.6 ± 4.5	20.8 ± 3.3	13.6 ± 8.1	17.6 ± 2.2	15.7 ± 2.3
SP4	10.4 ± 5.7	12.8 ± 6.0	15.0 ± 5.2	16.6 ± 4.9	18.9 ± 5.3	11.3 ± 1.9	12.4 ± 2.0	14.3 ± 2.5	16.2 ± 3.7	18.2 ± 3.2	8.9 ± 3.3	11.8 ± 2.4	10.2 ± 7.0	14.5 ± 2.9	15.0 ± 4.1
SP5	12.9 ± 5.8	15.0 ± 3.1	15.5 ± 3.1	14.3 ± 3.5	13.0 ± 2.9	10.4 ± 4.5	9.2 ± 2.9	9.2 ± 3.3	7.4 ± 3.5	7.2 ± 2.2	5.9 ± 1.6	5.1 ± 2.3	6.6 ± 7.5	2.8 ± 2.7	3.8 ± 2.9
SP6	1.2 ± 1.5	1.1 ± 1.8	0.9 ± 2.2	0.7 ± 1.1	0.8 ± 1.2	4.7 ± 4.3	5.6 ± 3.0	5.5 ± 2.9	6.1 ± 4.4	5.9 ± 3.3	9.4 ± 3.2	10.1 ± 3.1	10.7 ± 4.8	12.2 ± 2.6	11.8 ± 2.1
SP7	18.1 ± 5.0	15.1 ± 4.3	14.8 ± 3.8	14.6 ± 3.9	13.5 ± 3.7	19.8 ± 2.1	19.1 ± 2.5	17.7 ± 2.2	15.5 ± 2.6	14.5 ± 2.6	19.2 ± 3.5	18.1 ± 2.3	15.6 ± 6.9	15.8 ± 3.3	16.6 ± 3.3
SP8	10.7 ± 5.0	13.3 ± 5.3	14.7 ± 4.7	15.9 ± 5.5	18.8 ± 5.1	15.5 ± 2.6	15.0 ± 4.3	17.3 ± 6.8	19.7 ± 7.6	20.9 ± 8.8	7.1 ± 2.0	8.2 ± 3.0	8.5 ± 4.8	11.8 ± 6.1	12.6 ± 5.5
SP9	12.6 ± 6.9	13.1 ± 5.9	8.8 ± 5.4	7.8 ± 6.5	8.3 ± 6.2	15.0 ± 6.6	14.7 ± 5.2	12.2 ± 3.4	11.6 ± 4.1	8.7 ± 2.9	11.1 ± 4.3	7.3 ± 3.3	6.4 ± 7.1	4.1 ± 3.7	3.5 ± 3.4

Each value in the table is the mean ± SD percentage of individual support periods (SPs). Hemi1, first hemisection; Hemi2, second hemisection.

At Hemi1, the normalized burst amplitude was significantly smaller for RSRT ($P = 0.01$) and RECU ($P = 0.02$) compared to the intact state (Fig. 11, significant main effect of state). At Hemi2, these changes were no longer significantly different from the intact state. The LLG normalized amplitude did not change at Hemi1 but decreased at Hemi2 ($P = 0.04$). Although we found a significant main effect of state, pairwise comparisons showed no significant changes in normalized EMG burst amplitude for LSOL and LTRI after either hemisection compared to the intact state. We found that the normalized EMG burst amplitude remained unchanged across states for LBB, RBB, RTRI, LECU, LSRT, RSOL, and RLG (Fig. 11, no significant main effect of state).

DISCUSSION

The main goal of the present study was to determine how the locomotor pattern adjusts to different speeds on a treadmill after staggered thoracic lateral hemisections and to use kinematic and EMG data to assess changes in sensorimotor interactions. We found that the locomotor system compensates by reorganizing the temporal structure of the cycle in the hindlimbs across speeds, generating left-right asymmetries after the first hemisection that reverse after the second one. Below, we explain these compensatory changes to maintain speed modulation and the potential mechanisms involved based on our experimental data and our recent computational models (3, 19).

Left-Right Temporal Asymmetries Following Staggered Lateral Hemisections Are Due to Changes in Sensorimotor Interactions

After the first hemisection at T5–T6 on the right side, we observed shorter stance and longer swing phases in the ipsilesional right hindlimb compared to the contralesional left hindlimb across speeds (Fig. 4). This asymmetry reversed after the second hemisection on the left side at T10–T11, with shorter stance and longer swing in the left hindlimb compared to the right hindlimb. These asymmetries make functional sense because they favor a longer support period of the contralesional hindlimb after each lesion. After the first right hemisection, stance is prolonged in the left hindlimb, whereas after the second left hemisection, stance is prolonged in the right hindlimb. Interestingly, these compensatory changes were maintained across speeds and likely contributed to the reduction of support *periods 1* and *5*, which involve simultaneous support by both hindlimbs (Fig. 7). The changes in stance and swing phase durations that we observed at 7–8 wk after the first and second hemisections were undoubtedly due to the lesions. Audet et al. (26), using the same paradigm, albeit at a single speed of 0.4 m/s, showed similar changes/reversals in phase durations at an early time point (1–2 wk) after both hemisections that were maintained over time at 7–8 wk post lesions. Thus, it is unlikely that the main changes in phase durations were due to training and/or time-dependent effects.

What triggers this compensation? Is it a voluntary decision made by the animal or simply a consequence of the lesion based on network architecture? In our recent model, we proposed that supraspinal drive adjusts the gain of somatosensory feedback onto ipsilateral flexor and extensor half-centers

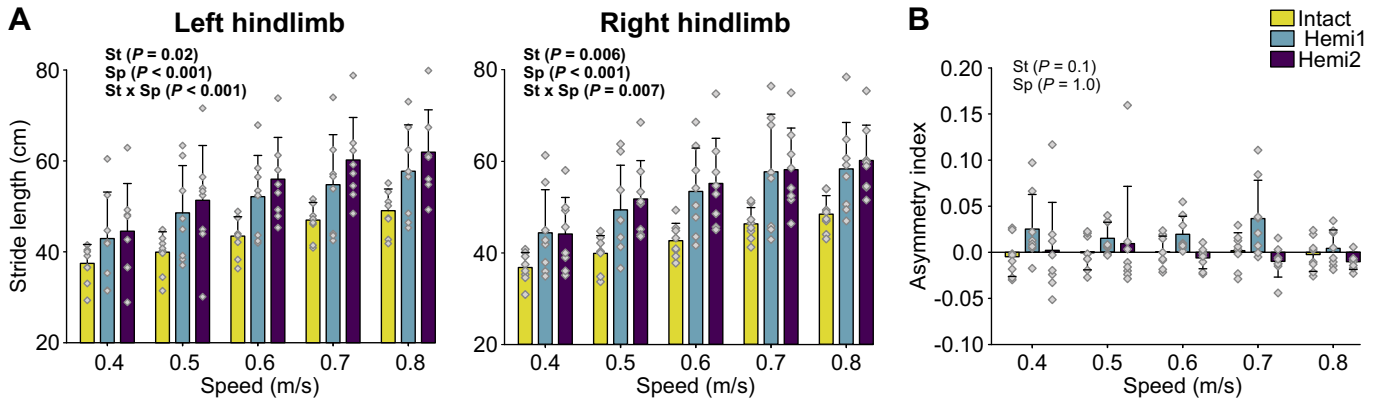

Figure 8. Stride lengths across speeds before and after staggered hemisections. *A*: bars represent the mean ± SD of stride lengths for the left and right hindlimbs ($n = 8$ cats), with light gray diamonds showing individual means. *B*: asymmetry index of right and left hindlimb stride lengths. Bars represent the mean ± SD ($n = 8$ cats). *P* values for the main effects of state (St), speed (Sp), and their interaction (St × Sp) were obtained from a linear mixed-effects model followed by a type III ANOVA and are shown atop each panel. *P* values in bold indicate a significant main effect at <0.05. Hemi1, first hemisection; Hemi2, second hemisection.

through presynaptic inhibition [see Fig. 1 of Rybak et al. (19)]. Several studies have shown or proposed a decrease in presynaptic inhibition after spinal cord injury (52–55), although a few studies have shown or suggested an increase (56, 57). Differences likely stem from different preparations and the indirect measures generally used to assess presynaptic inhibition.

In our model, somatosensory feedback includes stretch-related signals related to hip extension that excite the ipsilateral flexor half-center (27), which we termed SF-E1 in our model, as well as loading-dependent signals from limb extensor muscles that activate the ipsilateral extensor half-center, which we termed SF-E2 (58–60). Thus, the loss of supraspinal drive on the right side following the first hemisection reduces presynaptic inhibition of excitatory length inputs from hip flexor group Ia/II afferents to the flexor half-center, initiating an earlier stance-to-swing transition and thereby shortening stance and prolonging swing in the ipsilesional hindlimb. The supraspinal drive and its inhibition of SF-E2 are also abolished after hemisection. However, as stance is shortened on the side of the lesion, the time spent loading the limb and the influence of SF-E2 on the extensor half-center are also reduced. This earlier onset and prolongation of the swing phase increases inhibitory input on the contralateral flexor half-center through inhibitory connections between the right and left flexor half-centers via commissural interneurons. In addition, reduced presynaptic inhibition of ipsilesional length feedback SF-E1 on the right side increases excitatory input on the contralesional left extensor half-center. Reduced excitation of the left flexor half-center disinhibits the left extensor half-center and prolongs left stance. This allows both hindlimbs to maintain equal cycle duration. After the second hemisection on the left side the pattern is reversed, increasing left swing, decreasing left stance, decreasing right swing, and increasing right stance. Again, according to our model, this is a consequence of the lesion and the disinhibition of SF-E1 on the left side. We cannot exclude other scenarios or mechanisms, but this is a simple explanation based on network architecture. Although we did not find a significant increase in hip angle following staggered hemisections (Fig. 9), this is not necessary for an increased excitatory influence of SF-E1 onto the ipsilateral flexor half-center, which is mediated by disinhibition of SF-E1 due to the loss of supraspinal drive. However, the increase in hip angle at liftoff with increasing speed in the intact state, which was maintained after hemisections, serves to counteract the increased supraspinal drive and inhibition of SF-E1. Figure 12 schematically illustrates the main changes in sensorimotor interactions leading to left-right asymmetries in phase durations after staggered hemisections.

Changes in stance/extensor burst durations and swing/flexor burst durations after staggered hemisections also

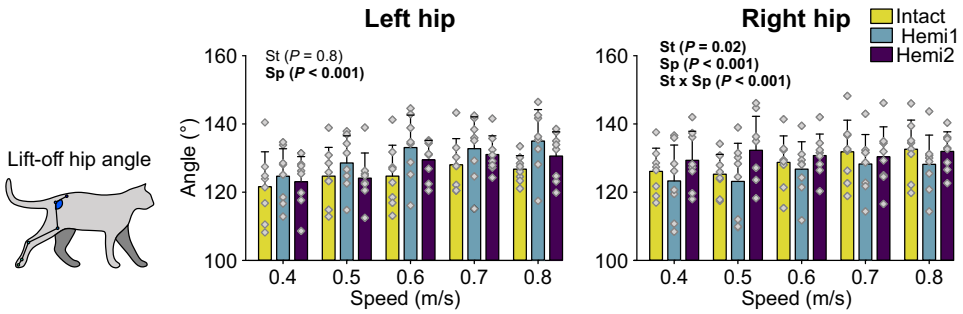

Figure 9. Hip angle at liftoff across speeds before and after staggered hemisections. Hip joint angles were measured at liftoff of the left and right hindlimbs before and after hemisections. Bars represent mean ± SD ($n = 8$ cats), with light gray diamonds indicating individual means. *P* values for the main effects of state (St), speed (Sp), and their interaction (St × Sp) were obtained from a linear mixed-effects model followed by a type III ANOVA and are shown atop each panel. *P* values in bold indicate a significant main effect at <0.05. Hemi1, first hemisection; Hemi2, second hemisection.

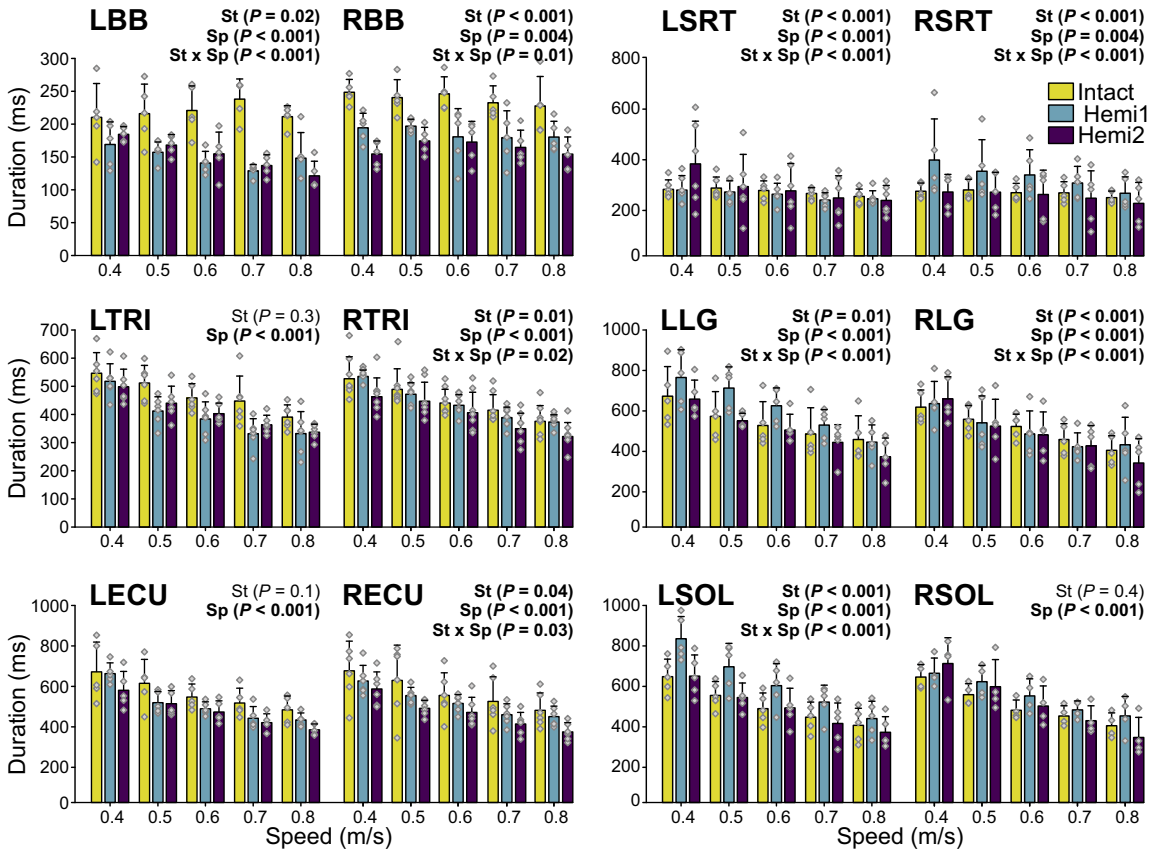

Figure 10. Electromyographic (EMG) burst duration in forelimb and hindlimb muscles across speeds before and after staggered hemisections. Bars represent means ± SD of EMG burst durations, with light gray diamonds showing means per individual cat. *P* values for the main effects of state (St), speed (Sp), and their interaction (St × Sp) were obtained from a linear mixed-effects model followed by a type III ANOVA and are shown atop each panel. *P* values in bold indicate a significant main effect at <0.05. Hemi1, first hemisection; Hemi2, second hemisection. L, left; R, right. BB, biceps brachii (RBB, $n = 5$; LBB, $n = 5$); ECU, extensor carpi ulnaris (RECU, $n = 6$; LECU, $n = 5$); LG, lateral gastrocnemius (RLG, $n = 5$; LLG, $n = 5$); SOL, soleus (RSOL, $n = 4$; LSOL, $n = 5$); SRT, sartorius (RSRT, $n = 5$; LSRT, $n = 6$); TRI, triceps brachii (RTRI, $n = 7$; LTRI, $n = 6$).

affected the control of cycle duration as a function of speed (Fig. 5). In the intact state, in all four limbs, cycle duration varied mainly with stance duration with a change in speed. This stance/extensor dominance has been demonstrated in several studies in cats and humans (10, 12, 37, 39, 40, 42–44). However, after the first hemisection, stance dominance weakened in the ipsilesional right hindlimb as cycle duration varied with both stance and swing durations, while the left hindlimb maintained stance dominance. These results align with previous findings in cats with a lateral thoracic hemisection (17) or lateral funiculi lesions (61). After the second hemisection on the left side, stance dominance weakened in the left hindlimb as cycle duration now varied with both stance and swing durations, and although stance dominance recovered in the right hindlimb, it did not return to intact values. For both hindlimbs, weakened stance dominance correlated with an increase in swing proportion (Fig. 6). Swing proportion increased in the right ipsilesional hindlimb after the first hemisection and remained elevated after the second, whereas in the left hindlimb it only increased after the second hemisection. Again, we propose that this is due to changes in sensorimotor interactions as described above (Fig. 12).

Studies have shown that variations in cycle and phase durations are sensitive to supraspinal inputs and somatosensory feedback (10, 34, 46–48). For instance, electrically stimulating the mesencephalic locomotor region during spontaneously occurring fictive locomotion can switch an extensor-dominated rhythm to a flexor-dominated one (46). Descending motor pathways running in the dorsolateral cord, such as the corticospinal and rubrospinal tracts, seem particularly important in regulating flexor/swing phase duration (45, 62). In contrast, descending pathways running in the ventral/ventrolateral funiculi, such as the reticulospinal and vestibulospinal tracts, appear essential for extensor activation and support (61, 63, 64). However, if supraspinal inputs significantly contribute to phase dominance, why do spinal cats maintain stance/extensor dominance during real and fictive locomotion (46, 65)? One study showed that stretching and/or loading ankle extensors, thus increasing group I/II afferent feedback from these muscles, strengthened extensor dominance (47). In the present study, we observed reduced activity in an ipsilesional ankle plantarflexor after the first (e.g., RLG) and second (e.g., LLG) hemisections (Fig. 11). Reduced group I/II feedback from extensor muscles on the side of the lesion could have weakened extensor dominance while an increase in RLG activity after the

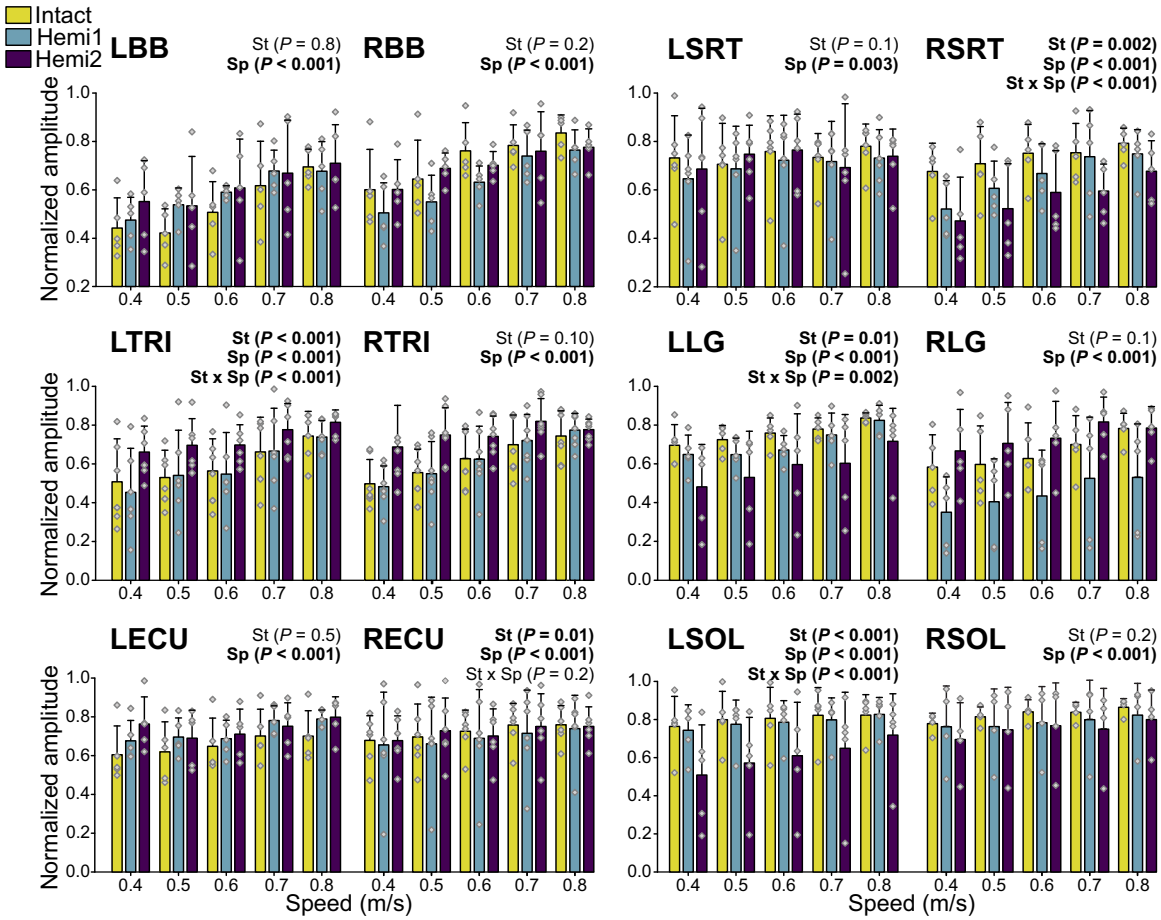

Figure 11. Normalized electromyographic (EMG) burst amplitudes in forelimb and hindlimb muscles across speeds before and after staggered hemisections. The amplitude of EMG signals was normalized to the value obtained at 0.8 m/s and analyzed for different muscles across speeds before and after hemisections. Bars represent means ± SD of EMG burst durations, with light gray diamonds showing means per individual cat. *P* values for the main effects of state (St), speed (Sp), and their interaction (St × Sp) were obtained from a linear mixed-effects model followed by a type III ANOVA and are shown atop each panel. *P* values in bold indicate a significant main effect at <0.05. Hemi1, first hemisection; Hemi2, second hemisection. L, left; R, right. BB, biceps brachii (RBB, $n = 5$; LBB, $n = 5$); ECU, extensor carpi ulnaris (RECU, $n = 6$; LECU, $n = 5$); LG, lateral gastrocnemius (RLG, $n = 5$; LLG, $n = 5$); SOL, soleus (RSOL, $n = 4$; LSOL, $n = 5$); SRT, sartorius (RSRT, $n = 5$; LSRT, $n = 6$); TRI, triceps brachii (RTRI, $n = 7$; LTRI, $n = 6$).

second left hemisection, reflecting increased loading of the right hindlimb, could have contributed to restoring right hindlimb extensor dominance. Split-belt locomotion in intact and spinal cats, which induces left-right asymmetries in sensory feedback from the hindlimbs, can also weaken stance/extensor dominance in the hindlimb stepping on the fast belt by shifting the center of mass toward the slower-moving belt (10, 66). Asymmetries in cutaneous sensory feedback from paw pads also induce left-right asymmetries by shifting the body weight toward the anesthetized paw during the stance phase in split-belt locomotion to maximize load-dependent sensory inputs (66). Thus, we think that the increase in swing/flexor dominance and/or weakened stance/extensor dominance is due to left-right asymmetries in supraspinal pathways and somatosensory feedback induced by the lesions, which do not occur after a complete transection.

On the other hand, we did not observe left-right asymmetries in stride lengths after staggered hemisections, and they continued to increase with speed while maintaining left-right symmetry (Fig. 8). Why is it that the temporal structure of the left-right pattern is reorganized but not the spatial one after staggered hemisections? Stride length reflects the distance traveled by the limb during the stance phase, added to the distance traveled by the treadmill during the swing phase (26, 30, 37, 38). Thus, stride length directly depends on speed and cycle duration because it is the product of treadmill speed and the sum of stance and swing phase durations. After hemisections, although stance and swing durations were asymmetrically modulated between the limbs, these changes occurred reciprocally, preserving symmetrical left-right cycle duration and thus maintaining equal left-right stride lengths. However, a limitation of using this formula after the injury is that it assumes continuous forward progression during the swing phase, as the distance traveled during the swing phase is calculated as the swing duration multiplied by the treadmill speed. But after hemisection, the swing trajectory might be altered (e.g., the limb may take longer to lift or pause at a certain point of the swing phase) so that the swing duration no longer reflects pure forward displacement.

Lesion Extent and Interanimal Variability

Performing a perfect lateral hemisection is not realistic, and the estimated amount of damaged pathways varied

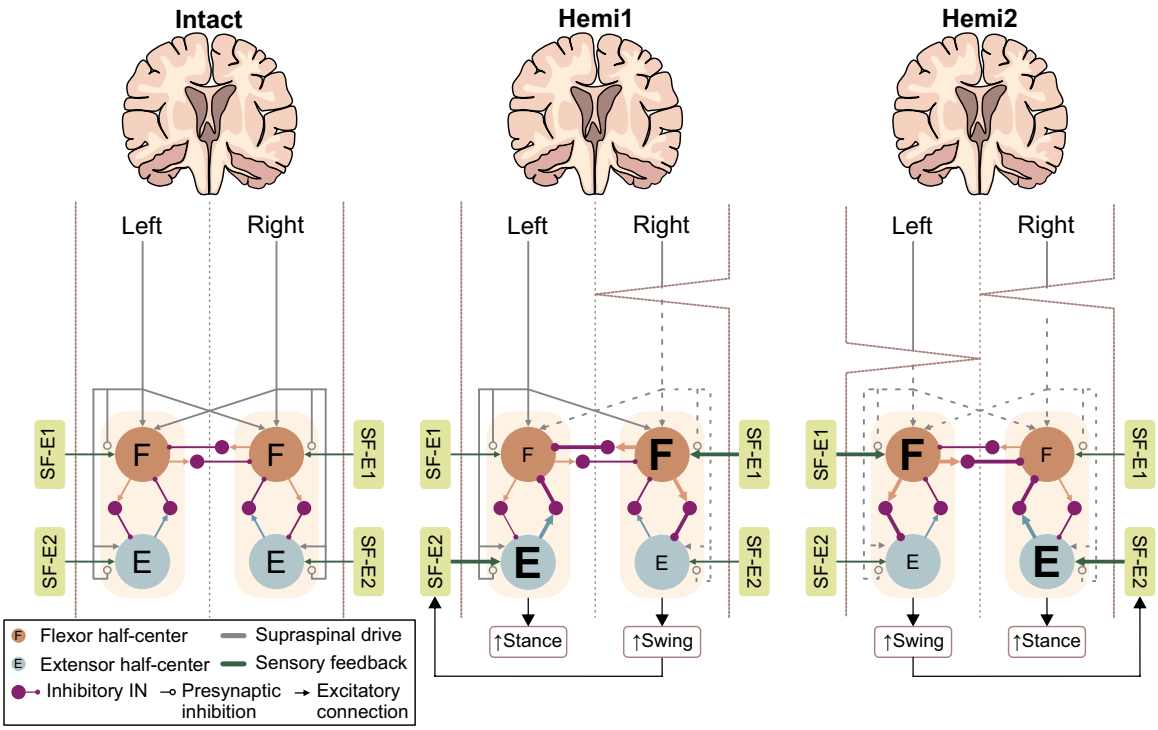

Figure 12. Schematic representation of the speed-dependent control of phase durations before and after staggered thoracic hemisections. The figure shows a simplified version of our published models [Rybak et al. (3), Rybak et al. (19)]. At the level of the spinal cord, rhythm generators, 1 for each hindlimb, are represented as extensor (E) and flexor (F) half-centers. The left and right F half-centers mutually inhibit each other via commissural inhibitory interneurons. The F half-center receives somatosensory feedback from hip flexor group Ia/II afferents (SF-E1), whereas the E half-center receives feedback from group Ib afferents (SF-E2). SF-E1 and SF-E2 are both active during the stance phase and are presynaptically inhibited by supraspinal drive. Supraspinal inputs send excitatory drive to both the F and E half-centers. After the first hemisection on the right side (Hemi1), supraspinal drive and its inhibition of SF-E1 and SF-E2 are abolished on the right. This leads to greater excitatory feedback from SF-E1 on the right F half-center. Because loading and thus SF-E2 are reduced for the right hindlimb, the excitatory effects of SF-E2 on the E half-center do not change much from the intact state, despite reduced presynaptic inhibition. After the second hemisection on the left side (Hemi2), the reverse occurs, with greater excitatory inputs from left SF-E1 onto the left F half-center. The effects on left and right stance and swing phases are described in the main text.

from one animal to another (Fig. 1). For instance, both hemisections typically damaged the lateral, dorsolateral, and ventrolateral funiculi, disrupting descending tracts such as the lateral corticospinal, rubrospinal, and medullary reticulospinal pathways on the lesioned side. These damaged pathways are involved in voluntary and postural control, as well as skilled movements and modulation of muscle activation (67–69). With the first hemisection, four cats (JA, HO, GR, PO) retained portions of the right ventral funiculus, preserving anterior corticospinal, pontine reticulospinal, and vestibulospinal tracts, which are implicated in controlling muscle tone, posture, balance, and coordinated movements (67, 69–71). Two cats (AR, GR) had unilateral damage of the right dorsal column, whereas the others (TO, JA, HO, MB, KA, PO) displayed bilateral or complete damage, disrupting ascending somatosensory feedback essential for locomotor adjustments. With the second hemisection, four cats (JA, HO, GR, PO) had unilateral damage of the left dorsal column, one cat (MB) had bilateral damage, and the remaining cats (TO, AR, KA) showed almost complete sparing. Some cats (AR, MB, GR, PO) also retained portions of the left ventral funiculus at T10–T11. This variability in spared versus damaged pathways across animals likely influenced quadrupedal locomotion and its adjustment to treadmill speed.

However, it is important to mention that interanimal variability and locomotor adjustments observed after staggered hemisections cannot be limited to lesion extent and to spared or damaged pathways. Even in the intact state, cats exhibit inherent variability in spinal locomotor circuitry, reflex modulation, and muscle activation patterns, shaped by factors such as genetic polymorphisms, physiology, morphology, and prior movement or learning experiences (72). Spinal cord injury further amplifies this variability by altering neuronal pathways in various ways across animals. As a result, cats may develop similar and/or unique compensatory strategies after injuries. This variation was also reported by the divergent changes observed between cats in cutaneous-induced reflex responses after staggered thoracic hemisections (24, 25). Hence, although the location and extent of lesions influence locomotor recovery, the adopted compensatory mechanism after the injury depends on multiple factors. Staggered hemisections involve a series of neuroplastic changes.

As discussed above, we observed left-right temporal changes in the hindlimb pattern after each hemisection. How does this reflect neuroplasticity within spinal sensorimotor circuits controlling the left and right hindlimbs? We acknowledge that the model proposed by Rybak et al. (19) and in Fig. 12 oversimplifies the underlying neurobiology. It does not account for neural plasticity, only for changes in left-right sensorimotor interactions resulting from the

lesions. A unilateral lesion of the thoracic cord, followed a few weeks later by a complete thoracic transection a few segments below, highlights that substantial plasticity occurs within circuits intrinsic to the lumbosacral cord after the first lesion in adult cats (15–18, 73). Indeed, hindlimb locomotion was expressed the day after the transection, a recovery that normally takes a minimum of 3 wk. Although the hindlimb on the side of the hemisection displays a more robust pattern after spinal transection, both hindlimbs express locomotion, consistent with bilateral neuroplasticity, albeit asymmetrical. A similar phenomenon was observed after staggered thoracic hemisections followed by a complete thoracic transection, where hindlimb locomotion was also observed the day after transection (26). These studies underscore that spinal sensorimotor circuits caudal to the lesions controlling hindlimb locomotion, including speed modulation, become more autonomous and less reliant on supraspinal pathways after thoracic lesions. Martinez et al. (17) reported that covariations in stance and swing phase durations across speeds persisted in the hemisected hindlimb after complete spinal transection, consistent with a memory trace in the circuits controlling the hindlimb on the hemisected side. In the present study, the second hemisection on the left side partially restored stance dominance in the right hindlimb, the side of the first hemisection. Thus, spinal sensorimotor circuits retain the ability to induce left-right asymmetrical neuroplastic changes after a lateral hemisection in an already injured spinal cord.

Multiple mechanisms could have been involved in locomotor recovery after lateral hemisections performed on opposite sides of the spinal cord. In mice, a study comparing simultaneous versus temporally staggered thoracic lateral hemisections reported limited locomotor recovery after simultaneous lesions, restricted to the hindlimb ipsilateral to the first injury (22). In contrast, hemisections separated in time, as in the present study, allowed recovery of locomotion in both hindlimbs, suggesting that hindlimb recovery relies on time-dependent changes (22). Studies indicate that signal transmission between supraspinal and spinal circuits remains feasible after lateral hemisections on both sides of the cord, despite bilateral disruption of direct descending projections (22–24, 74–76). It has been proposed that propriospinal neurons form new circuits to allow for neural transmission across the two lesions (76, 77). Spared reticulospinal tracts sprout and appear to facilitate locomotor recovery in rats after incomplete SCI (78). In cats, spinal circuits also undergo substantial reorganization. After a right lateral hemisection, transmission between cervical and lumbar segments improves over time, as evidenced by the partial recovery of homolateral and diagonal cutaneous reflex responses after stimulation of the left superficial radial nerve (24). Beyond propriospinal plasticity, reorganization of primary afferent projections and local reflex circuits below the lesion may further contribute to locomotor recovery (79, 80). For example, proprioceptive afferents reorganize their synaptic connectivity with specific spinal targets and facilitate the formation and strengthening of descending circuits following thoracic hemisection (80, 81). Although our findings strongly suggest that reorganization within sensorimotor circuits caudal to the lesions plays a major role in locomotor recovery, multiple mechanisms are undoubtedly involved. Although the discussed neuroplastic changes might improve functional transmission between locomotor structures, they can exert both beneficial and detrimental effects on locomotion (75, 82–84). Future modeling efforts should incorporate or consider these multiple layers of plasticity, including cellular and molecular mechanisms. However, just because a new pathway transmits a neural signal or axonal sprouting occurs does not mean that they make a meaningful contribution to locomotor control.

Altered Forelimb-Hindlimb Coordination Following Staggered Thoracic Hemisections

Several studies have reported a 2:1 fore-hind pattern after SCIs in rats and cats (15, 26, 38, 61, 85–89). However, the mechanisms underlying this altered coordination are poorly understood. Fictive locomotion studies in decerebrate spinal cats have demonstrated that C3–C4 propriospinal neurons can generate rhythmic activity independently of lumbar and supraspinal inputs, supporting the existence of autonomous cervical central pattern generators (CPGs) (90). However, experimental evidence showed that the hindlimbs impose their rhythm on the forelimbs via ascending propriospinal pathways projecting from the lumbar to the cervical cord (91–93). After thoracic hemisections, these ascending pathways are disrupted and the hindlimbs' influence on the forelimbs is eliminated. Consequently, forelimb-hindlimb coordination is altered, and a 2:1 fore-hind pattern emerges. Despite this dissociation, 1:1 left-right coordination remains at both girdles, likely because of robust commissural interactions at cervical and lumbar levels. As mentioned above, a lateral hemisection reduces the excitatory supraspinal drive to the ipsilesional extensor half-center, shortening the stance phase and impairing hindlimb support. This biomechanical deficit shifts the center of mass rostrally, increasing the load on the forelimbs (87). One proposed mechanism to enhance stability after injury is to increase the forelimb cadence by shortening cycle duration and stride length to maintain the center of mass within the support polygon (94). Thus, the emergence of a 2:1 fore-hind pattern may contribute to this stabilizing strategy by expanding the support polygon (38). This further prevents interference between homolateral limb pairs, as evidenced by the increased frequency of diagonal support periods after the hemisections (Fig. 7). Finally, after a lateral thoracic hemisection, hindlimb locomotor activity depends more on somatosensory feedback and intrinsic spinal mechanisms (71). In contrast, cervical locomotor networks continue to receive excitatory supraspinal inputs and somatosensory feedback. However, the greater load demands on the forelimbs, and hence greater inputs from SF-E2 afferents, and the injury-related loss of ascending inhibitory inputs from hindlimb locomotor networks increase the excitability of forelimb CPGs, which increases their oscillatory rhythm and step frequency (87). Interactions between forelimb and hindlimb locomotor networks will need to be incorporated or considered in future modeling efforts.

Conclusions

In this study, we showed that locomotor adjustments to increasing treadmill speeds following thoracic staggered

hemisections involve a reorganization of the temporal structure of the locomotor cycle in both hindlimbs. Although these adjustments generate left-right temporal phase asymmetries that reverse after a second contralateral lesion, they maintain symmetrical cycle durations and stride lengths. This suggests the implication of compensatory mechanisms based on how the architecture of the network is organized and reorganized after spinal lesions (19). Understanding how speed is controlled after SCI in animal models is important from a translational perspective because people with SCI have difficulty attaining moderate walking speeds (4–8). Our findings underscore that locomotor circuit reorganization after SCI, including altered somatosensory feedback and reduced supraspinal drive, plays a key role in adjusting the locomotor pattern to speed variations.

DATA AVAILABILITY

The datasets generated and/or analyzed during the present study are available from the corresponding author on reasonable request.

ACKNOWLEDGMENTS

We thank Philippe Drapeau for providing data acquisition and analysis software, developed in the Rossignol and Drew laboratories at the Université de Montréal. We thank Louis Gendron and Claudie Beaulieu for conducting the histological analysis. We also thank the Biostatistics departments of the Centre de Recherche de Centre Hospitalier Universitaire de Sherbrooke for statistical assistance.

GRANTS

This work was supported by grants from the Natural Sciences and Engineering Research Council of Canada (NSERC RGPIN-2016–03790) to A.F. and from the National Institutes of Health (R01 NS110550) to A.F., I.A.R., and B.I.P. J.H. and A.N.M. were supported by Fonds de Recherche-Santé Quebec doctoral and postdoctoral scholarships, respectively. J.A. was supported by a doctoral scholarship from the Canadian Institutes of Health Research.

DISCLOSURES

No conflicts of interest, financial or otherwise, are declared by the authors.

AUTHOR CONTRIBUTIONS

I.A.R., B.I.P., and A.F. conceived and designed research; S.Y., J.A., C.G.L., S.M., A.N.M., and J.H. performed experiments; S.Y. and J.A. analyzed data; S.Y. and A.F. interpreted results of experiments; S.Y. prepared figures; S.Y. and A.F. drafted manuscript; S.Y., J.A., C.G.L., S.M., A.N.M., J.H., I.A.R., B.I.P., and A.F. edited and revised manuscript; S.Y., J.A., C.G.L., S.M., A.N.M., J.H., I.A.R., B.I.P., and A.F. approved final version of manuscript.

REFERENCES

1. **Rossignol S**, **Dubuc R**, **Gossard J.** Dynamic sensorimotor interactions in locomotion. *Physiol Rev* 86: 89–154, 2006. doi:10.1152/physrev.00028.2005.
2. **Frigon A**, **Akay T**, **Prilutsky BI.** Control of mammalian locomotion by somatosensory feedback. *Compr Physiol* 12: 2877–2947, 2021. doi:10.1002/j.2040-4603.2022.tb00203.x.
3. **Rybak IA**, **Shevtsova NA**, **Markin SN**, **Prilutsky BI**, **Frigon A.** Operation regimes of spinal circuits controlling locomotion and role of supraspinal drives and sensory feedback (Preprint). *bioRxiv* 2024.03.21.586122, 2024. doi:10.1101/2024.03.21.586122.
4. **Awai L**, **Bolliger M**, **Ferguson AR**, **Courtine G**, **Curt A.** Influence of spinal cord integrity on gait control in human spinal cord injury. *Neurorehabil Neural Repair* 30: 562–572, 2016. doi:10.1177/1545968315600524.
5. **Pépin A**, **Ladouceur M**, **Barbeau H.** Treadmill walking in incomplete spinal-cord-injured subjects: 2. Factors limiting the maximal speed. *Spinal Cord* 41: 271–279, 2003. doi:10.1038/sj.sc.3101453.
6. **Pépin A**, **Norman KE**, **Barbeau H.** Treadmill walking in incomplete spinal-cord-injured subjects: 1. Adaptation to changes in speed. *Spinal Cord* 41: 257–270, 2003. doi:10.1038/sj.sc.3101452.
7. **van Hedel HJ**; **EMSCI Study Group.** Gait speed in relation to categories of functional ambulation after spinal cord injury. *Neurorehabil Neural Repair* 23: 343–350, 2009. doi:10.1177/1545968308324224.
8. **van Hedel HJ**, **Dietz V**, **Curt A.** Assessment of walking speed and distance in subjects with an incomplete spinal cord injury. *Neurorehabil Neural Repair* 21: 295–301, 2007. doi:10.1177/1545968306297861.
9. **Barbeau H**, **Rossignol S.** Recovery of locomotion after chronic spinalization in the adult cat. *Brain Res* 412: 84–95, 1987. doi:10.1016/0006-8993(87)91442-9.
10. **Frigon A**, **Hurteau MF**, **Thibaudier Y**, **Leblond H**, **Telonio A**, **D'Angelo G.** Split-belt walking alters the relationship between locomotor phases and cycle duration across speeds in intact and chronic spinalized adult cats. *J Neurosci* 33: 8559–8566, 2013. doi:10.1523/JNEUROSCI.3931-12.2013.
11. **Frigon A**, **Desrochers É**, **Thibaudier Y**, **Hurteau M**, **Dambreville C.** Left-right coordination from simple to extreme conditions during split-belt locomotion in the chronic spinal adult cat. *J Physiol* 595: 341–361, 2017. doi:10.1113/JP272740.
12. **Harnie J**, **Audet J**, **Mari S**, **Lecomte CG**, **Merlet AN**, **Genois G**, **Rybak IA**, **Prilutsky BI**, **Frigon A.** State- and condition-dependent modulation of the hindlimb locomotor pattern in intact and spinal cats across speeds. *Front Syst Neurosci* 16: 814028, 2022. doi:10.3389/fnsys.2022.814028.
13. **Audet J**, **Harnie J**, **Lecomte CG**, **Mari S**, **Merlet AN**, **Prilutsky BI**, **Rybak IA**, **Frigon A.** Control of forelimb and hindlimb movements and their coordination during quadrupedal locomotion across speeds in adult spinal cats. *J Neurotrauma* 39: 1113–1131, 2022. doi:10.1089/neu.2022.0042.
14. **Rowald A**, **Komi S**, **Demesmaeker R**, **Baaklini E**, **Hernandez-Charpak SD**, **Paoles E**, **et al.** Activity-dependent spinal cord neuromodulation rapidly restores trunk and leg motor functions after complete paralysis. *Nat Med* 28: 260–271, 2022. doi:10.1038/s41591-021-01663-5.
15. **Barrière G**, **Frigon A**, **Leblond H**, **Provencher J**, **Rossignol S.** Dual spinal lesion paradigm in the cat: evolution of the kinematic locomotor pattern. *J Neurophysiol* 104: 1119–1133, 2010. doi:10.1152/jn.00255.2010.
16. **Martinez M**, **Delivet-Mongrain H**, **Leblond H**, **Rossignol S.** Recovery of hindlimb locomotion after incomplete spinal cord injury in the cat involves spontaneous compensatory changes within the spinal locomotor circuitry. *J Neurophysiol* 106: 1969–1984, 2011. doi:10.1152/jn.00368.2011.
17. **Martinez M**, **Delivet-Mongrain H**, **Leblond H**, **Rossignol S.** Incomplete spinal cord injury promotes durable functional changes within the spinal locomotor circuitry. *J Neurophysiol* 108: 124–134, 2012. doi:10.1152/jn.00073.2012.
18. **Barrière G**, **Leblond H**, **Provencher J**, **Rossignol S.** Prominent role of the spinal central pattern generator in the recovery of locomotion after partial spinal cord injuries. *J Neurosci* 28: 3976–3987, 2008. doi:10.1523/JNEUROSCI.5692-07.2008.
19. **Rybak IA**, **Shevtsova NA**, **Audet J**, **Yassine S**, **Markin SN**, **Prilutsky BI**, **Frigon A.** Operation of spinal sensorimotor circuits controlling phase durations during tied-belt and split-belt locomotion after a lateral thoracic hemisection. *eLife* 13: RP103504, 2025. doi:10.7554/eLife.103504.3.
20. **Hopcroft JE**, **Motwani R**, **Ullman JD.** Introduction to automata theory, languages, and computation, 2nd edition. *SIGACT News* 32: 60–65, 2001. doi:10.1145/568438.568455.
21. **Wang J.** *Formal Methods in Computer Science*. Chapman and Hall/CRC, 2019.
22. **Courtine G**, **Song B**, **Roy RR**, **Zhong H**, **Herrmann JE**, **Ao Y**, **Qi J**, **Edgerton VR**, **Sofroniew MV.** Recovery of supraspinal control of

stepping via indirect propriospinal relay connections after spinal cord injury. *Nat Med* 14: 69–74, 2008.
23. **Cowley KC**, **MacNeil BJ**, **Chopek JW**, **Sutherland S**, **Schmidt BJ.** Neurochemical excitation of thoracic propriospinal neurons improves hindlimb stepping in adult rats with spinal cord lesions. *Exp Neurol* 264: 174–187, 2015. doi:10.1016/j.expneurol.2014.12.006.
24. **Mari S**, **Lecomte CG**, **Merlet AN**, **Audet J**, **Yassine S**, **Arab RA**, **Harnie J**, **Rybak IA**, **Prilutsky BI**, **Frigon A.** Changes in intra- and interlimb reflexes from forelimb cutaneous afferents after staggered thoracic lateral hemisections during locomotion in cats. *J Physiol* 602: 6225–6258, 2024. doi:10.1113/JP286808.
25. **Mari S**, **Lecomte CG**, **Merlet AN**, **Audet J**, **Yassine S**, **Eddaoui O**, **Genois G**, **Nadeau C**, **Harnie J**, **Rybak IA**, **Prilutsky BI**, **Frigon A.** Changes in intra- and interlimb reflexes from hindlimb cutaneous afferents after staggered thoracic lateral hemisections during locomotion in cats. *J Physiol* 602: 1987–2017, 2024. doi:10.1113/JP286151.
26. **Audet J**, **Yassine S**, **Lecomte CG**, **Mari S**, **Soucy F**, **Morency C**, **Merlet AN**, **Harnie J**, **Beaulieu C**, **Gendron L**, **Rybak IA**, **Prilutsky BI**, **Frigon A.** Spinal sensorimotor circuits play a prominent role in hindlimb locomotor recovery after staggered thoracic lateral hemisections but cannot restore posture and interlimb coordination during quadrupedal locomotion in adult cats. *eNeuro* 10: ENEURO.0191-23.2023, 2023. doi:10.1523/ENEURO.0191-23.2023.
27. **Grillner S**, **Rossignol S.** On the initiation of the swing phase of locomotion in chronic spinal cats. *Brain Res* 146: 269–277, 1978. doi:10.1016/0006-8993(78)90973-3.
28. **Duysens J**, **Pearson KG.** Inhibition of flexor burst generation by loading ankle extensor muscles in walking cats. *Brain Res* 187: 321–332, 1980. doi:10.1016/0006-8993(80)90206-1.
29. **Merlet AN**, **Jéhannin P**, **Mari S**, **Lecomte CG**, **Audet J**, **Harnie J**, **Rybak IA**, **Prilutsky BI**, **Frigon A.** Sensory perturbations from hindlimb cutaneous afferents generate coordinated functional responses in all four limbs during locomotion in intact cats. *eNeuro* 9: ENEURO.0178-22.2022, 2022. doi:10.1523/ENEURO.0178-22.2022.
30. **Lecomte CG**, **Mari S**, **Audet J**, **Merlet AN**, **Harnie J**, **Beaulieu C**, **Abdallah K**, **Gendron L**, **Rybak IA**, **Prilutsky BI**, **Frigon A.** Modulation of the gait pattern during split-belt locomotion after lateral spinal cord hemisection in adult cats. *J Neurophysiol* 128: 1593–1616, 2022. doi:10.1152/jn.00230.2022.
31. **Mari S**, **Lecomte CG**, **Merlet AN**, **Audet J**, **Harnie J**, **Rybak IA**, **Prilutsky BI**, **Frigon A.** A sensory signal related to left-right symmetry modulates intra- and interlimb cutaneous reflexes during locomotion in intact cats. *Front Syst Neurosci* 17: 1199079, 2023. doi:10.3389/fnsys.2023.1199079.
32. **Lecomte CG**, **Mari S**, **Audet J**, **Yassine S**, **Merlet AN**, **Morency C**, **Harnie J**, **Beaulieu C**, **Gendron L**, **Frigon A.** Neuromechanical strategies for obstacle negotiation during overground locomotion following incomplete spinal cord injury in adult cats. *J Neurosci* 43: 5623–5641, 2023. doi:10.1523/JNEUROSCI.0478-23.2023.
33. **Merlet AN**, **Harnie J**, **Frigon A.** Inhibition and facilitation of the spinal locomotor central pattern generator and reflex circuits by somatosensory feedback from the lumbar and perineal regions after spinal cord injury. *Front Neurosci* 15: 720542, 2021. doi:10.3389/fnins.2021.720542.
34. **Frigon A**, **D'Angelo G**, **Thibaudier Y**, **Hurteau MF**, **Telonio A**, **Kuczynski V**, **Dambreville C.** Speed-dependent modulation of phase variations on a step-by-step basis and its impact on the consistency of interlimb coordination during quadrupedal locomotion in intact adult cats. *J Neurophysiol* 111: 1885–1902, 2014. doi:10.1152/jn.00524.2013.
35. **Wetzel MC**, **Stuart DG.** Ensemble characteristics of cat locomotion and its neural control. *Prog Neurobiol* 7: 1–98, 1976. doi:10.1016/0301-0082(76)90002-2.
36. **Mathis A**, **Mamidanna P**, **Cury KM**, **Abe T**, **Murthy VN**, **Mathis MW**, **Bethge M.** DeepLabCut: markerless pose estimation of user-defined body parts with deep learning. *Nat Neurosci* 21: 1281–1289, 2018. doi:10.1038/s41593-018-0209-y.
37. **Dambreville C**, **Labarre A**, **Thibaudier Y**, **Hurteau MF**, **Frigon A.** The spinal control of locomotion and step-to-step variability in left-right symmetry from slow to moderate speeds. *J Neurophysiol* 114: 1119–1128, 2015. doi:10.1152/jn.00419.2015.
38. **Thibaudier Y**, **Hurteau M**, **Dambreville C**, **Chraibi A**, **Goetz L**, **Frigon A.** Interlimb Coordination during tied-belt and transverse split-belt locomotion before and after an incomplete spinal cord injury. *J Neurotrauma* 34: 1751–1765, 2017. doi:10.1089/neu.2016.4421.
39. **Goslow GE, Jr.**, **Reinking RM**, **Stuart DG.** The cat step cycle: hind limb joint angles and muscle lengths during unrestrained locomotion. *J Morphol* 141: 1–41, 1973. doi:10.1002/jmor.1051410102.
40. **Grillner S**, **Halbertsma J**, **Nilsson J**, **Thorstensson A.** The adaptation to speed in human locomotion. *Brain Res* 165: 177–182, 1979. doi:10.1016/0006-8993(79)90059-3.
41. **Halbertsma JM.** The stride cycle of the cat: the modelling of locomotion by computerized analysis of automatic recordings. *Acta Physiol Scand Suppl* 521: 1–75, 1983.
42. **Gossard JP**, **Sirois J**, **Noué P**, **Côté MP**, **Ménard A**, **Leblond H**, **Frigon A.** Chapter 2–the spinal generation of phases and cycle duration. *Prog Brain Res* 188: 15–29, 2011. doi:10.1016/B978-0-444-53825-3.00007-3.
43. **Frigon A.** Central pattern generators of the mammalian spinal cord. *Neuroscientist* 18: 56–69, 2012. doi:10.1177/1073858410396101.
44. **Harnie J**, **Côté-Sarrazin C**, **Hurteau MF**, **Desrochers E**, **Doelman A**, **Amhis N**, **Frigon A.** The modulation of locomotor speed is maintained following partial denervation of ankle extensors in spinal cats. *J Neurophysiol* 120: 1274–1285, 2018. doi:10.1152/jn.00812.2017.
45. **Yakovenko S**, **McCrea DA**, **Stecina K**, **Prochazka A.** Control of locomotor cycle durations. *J Neurophysiol* 94: 1057–1065, 2005. doi:10.1152/jn.00991.2004.
46. **Frigon A**, **Gossard JP.** Asymmetric control of cycle period by the spinal locomotor rhythm generator in the adult cat. *J Physiol* 587: 4617–4628, 2009. doi:10.1113/jphysiol.2009.176669.
47. **Frigon A**, **Gossard JP.** Evidence for specialized rhythm-generating mechanisms in the adult mammalian spinal cord. *J Neurosci* 30: 7061–7071, 2010. doi:10.1523/JNEUROSCI.0450-10.2010.
48. **D'Angelo G**, **Thibaudier Y**, **Telonio A**, **Hurteau M-F**, **Kuczynski V**, **Dambreville C**, **Frigon A.** Modulation of phase durations, phase variations, and temporal coordination of the four limbs during quadrupedal split-belt locomotion in intact adult cats. *J Neurophysiol* 112: 1825–1837, 2014. doi:10.1152/jn.00160.2014.
49. **Błaszczyk JW**, **Dobrzecka C.** Speed control in quadrupedal locomotion: principles of limb coordination in the dog. *Acta Neurobiol Exp (Wars)* 49: 105–124, 1989.
50. **Courtine G**, **Roy RR**, **Hodgson J**, **McKay H**, **Raven J**, **Zhong H**, **Yang H**, **Tuszynski MH**, **Edgerton VR.** Kinematic and EMG determinants in quadrupedal locomotion of a non-human primate (Rhesus). *J Neurophysiol* 93: 3127–3145, 2005. doi:10.1152/jn.01073.2004.
51. **Kriellaars DJ**, **Brownstone RM**, **Noga BR**, **Jordan LM.** Mechanical entrainment of fictive locomotion in the decerebrate cat. *J Neurophysiol* 71: 2074–2086, 1994. doi:10.1152/jn.1994.71.6.2074.
52. **Naftchi NE**, **Schlosser W**, **Horst WD.** Correlation of changes in the GABA-ergic system with the development of spasticity in paraplegic cats. *Adv Exp Med Biol* 123: 431–450, 1979. doi:10.1007/978-1-4899-5199-1_27.
53. **Lalonde NR**, **Bui TV.** Do spinal circuits still require gating of sensory information by presynaptic inhibition after spinal cord injury? *Curr Opin Physiol* 19: 113–118, 2021. doi:10.1016/j.cophys.2020.10.001.
54. **Calancie B**, **Broton JG**, **Klose KJ**, **Traad M**, **Difini J**, **Ayyar DR.** Evidence that alterations in presynaptic inhibition contribute to segmental hypo- and hyperexcitability after spinal cord injury in man. *Electroencephalogr Clin Neurophysiol* 89: 177–186, 1993. doi:10.1016/0168-5597(93)90131-8.
55. **Caron G**, **Bilchak JN**, **Côté MP.** Direct evidence for decreased presynaptic inhibition evoked by PBSt group I muscle afferents after chronic SCI and recovery with step-training in rats. *J Physiol* 598: 4621–4642, 2020. doi:10.1113/JP280070.
56. **Hultborn H**, **Malmsten J.** Changes in segmental reflexes following chronic spinal cord hemisection in the cat. II. Conditioned monosynaptic test reflexes. *Acta Physiol Scand* 119: 423–433, 1983. doi:10.1111/j.1748-1716.1983.tb07358.x.
57. **Hultborn H**, **Malmsten J.** Changes in segmental reflexes following chronic spinal cord hemisection in the cat. I. Increased monosynaptic and polysynaptic ventral root discharges. *Acta Physiol Scand* 119: 405–422, 1983. doi:10.1111/j.1748-1716.1983.tb07357.x.
58. **Conway BA**, **Hultborn H**, **Kiehn O.** Proprioceptive input resets central locomotor rhythm in the spinal cat. *Exp Brain Res* 68: 643–656, 1987. doi:10.1007/BF00249807.
59. **Gossard JP**, **Brownstone RM**, **Barajon I**, **Hultborn H.** Transmission in a locomotor-related group Ib pathway from hindlimb extensor

muscles in the cat. *Exp Brain Res* 98: 213–228, 1994. doi:10.1007/BF00228410.
60. **Pearson KG**, **Collins DF.** Reversal of the influence of group Ib afferents from plantaris on activity in medial gastrocnemius muscle during locomotor activity. *J Neurophysiol* 70: 1009–1017, 1993. doi:10.1152/jn.1993.70.3.1009.
61. **Górska T**, **Bem T**, **Majczyński H**, **Zmysłowski W.** Unrestrained walking in cats with partial spinal lesions. *Brain Res Bull* 32: 241–249, 1993. doi:10.1016/0361-9230(93)90183-c.
62. **Bretzner F**, **Drew T.** Contribution of the motor cortex to the structure and the timing of hindlimb locomotion in the cat: a microstimulation study. *J Neurophysiol* 94: 657–672, 2005. doi:10.1152/jn.01245.2004.
63. **Orlovsky GN.** Activity of vestibulospinal neurons during locomotion. *Brain Res* 46: 85–98, 1972. doi:10.1016/0006-8993(72)90007-8.
64. **Mori S.** Contribution of postural muscle tone to full expression of posture and locomotor movements: multi-faceted analyses of its setting brainstem-spinal cord mechanisms in the cat. *Jpn J Physiol* 39: 785–809, 1989. doi:10.2170/jjphysiol.39.785.
65. **Grillner S**, **Zangger P.** On the central generation of locomotion in the low spinal cat. *Exp Brain Res* 34: 241–261, 1979. doi:10.1007/BF00235671.
66. **Park H**, **Latash EM**, **Molkov YI**, **Klishko AN**, **Frigon A**, **DeWeerth SP**, **Prilutsky BI.** Cutaneous sensory feedback from paw pads affects lateral balance control during split-belt locomotion in the cat. *J Exp Biol* 222: jeb198648, 2019. doi:10.1242/jeb.198648.
67. **Cho TA.** Spinal cord functional anatomy. *Continuum (Minneap Minn)* 21: 13–35, 2015. doi:10.1212/01.CON.0000461082.25876.4a.
68. **Natali AL**, **Reddy V**, **Bordoni B.** Neuroanatomy, corticospinal cord tract. In: *StatPearls*. StatPearls Publishing, 2025.
69. **Lemon RN.** Descending pathways in motor control. *Annu Rev Neurosci* 31: 195–218, 2008. doi:10.1146/annurev.neuro.31.060407.125547.
70. **Field-Fote EC**, **Yang JF**, **Basso DM**, **Gorassini MA.** Supraspinal control predicts locomotor function and forecasts responsiveness to training after spinal cord injury. *J Neurotrauma* 34: 1813–1825, 2017. doi:10.1089/neu.2016.4565.
71. **Frigon A.** The neural control of interlimb coordination during mammalian locomotion. *J Neurophysiol* 117: 2224–2241, 2017. doi:10.1152/jn.00978.2016.
72. **Frigon A.** Chapter 7–interindividual variability and its implications for locomotor adaptation following peripheral nerve and/or spinal cord injury. *Prog Brain Res* 188: 101–118, 2011. doi:10.1016/B978-0-444-53825-3.00012-7.
73. **Rossignol S**, **Frigon A.** Recovery of locomotion after spinal cord injury: some facts and mechanisms. *Annu Rev Neurosci* 34: 413–440, 2011. doi:10.1146/annurev-neuro-061010-113746.
74. **Cowley KC**, **Zaporozhets E**, **Schmidt BJ.** Propriospinal neurons are sufficient for bulbospinal transmission of the locomotor command signal in the neonatal rat spinal cord. *J Physiol* 586: 1623–1635, 2008. doi:10.1113/jphysiol.2007.148361.
75. **Anderson MA**, **Squair JW**, **Gautier M**, **Hutson TH**, **Kathe C**, **Barraud Q**, **Bloch J**, **Courtine G.** Natural and targeted circuit reorganization after spinal cord injury. *Nat Neurosci* 25: 1584–1596, 2022. doi:10.1038/s41593-022-01196-1.
76. **Bareyre FM**, **Kerschensteiner M**, **Raineteau O**, **Mettenleiter TC**, **Weinmann O**, **Schwab ME.** The injured spinal cord spontaneously forms a new intraspinal circuit in adult rats. *Nat Neurosci* 7: 269–277, 2004. doi:10.1038/nn1195.
77. **Fouad K**, **Pedersen V**, **Schwab ME**, **Brösamle C.** Cervical sprouting of corticospinal fibers after thoracic spinal cord injury accompanies shifts in evoked motor responses. *Curr Biol* 11: 1766–1770, 2001. doi:10.1016/S0960-9822(01)00535-8.
78. **Ballermann M**, **Fouad K.** Spontaneous locomotor recovery in spinal cord injured rats is accompanied by anatomical plasticity of reticulospinal fibers. *Eur J Neurosci* 23: 1988–1996, 2006. doi:10.1111/j.1460-9568.2006.04726.x.
79. **Helgren ME**, **Goldberger ME.** The recovery of postural reflexes and locomotion following low thoracic hemisection in adult cats involves compensation by undamaged primary afferent pathways. *Exp Neurol* 123: 17–34, 1993. doi:10.1006/exnr.1993.1137.
80. **Takeoka A**, **Arber S.** Functional local proprioceptive feedback circuits initiate and maintain locomotor recovery after spinal cord injury. *Cell Rep* 27: 71–85.e3, 2019. doi:10.1016/j.celrep.2019.03.010.
81. **Takeoka A**, **Vollenweider I**, **Courtine G**, **Arber S.** Muscle spindle feedback directs locomotor recovery and circuit reorganization after spinal cord injury. *Cell* 159: 1626–1639, 2014. doi:10.1016/j.cell.2014.11.019.
82. **Shepard CT**, **Brown BL**, **Van Rijswijck MA**, **Zalla RM**, **Burke DA**, **Morehouse JR**, **Riegler AS**, **Whittemore SR**, **Magnuson DS.** Silencing long-descending inter-enlargement propriospinal neurons improves hindlimb stepping after contusive spinal cord injuries. *eLife* 12: e82944, 2023. doi:10.7554/eLife.82944.
83. **Shepard CT**, **Pocratsky AM**, **Brown BL**, **Van Rijswijck MA**, **Zalla RM**, **Burke DA**, **Morehouse JR**, **Riegler AS**, **Whittemore SR**, **Magnuson DS.** Silencing long ascending propriospinal neurons after spinal cord injury improves hindlimb stepping in the adult rat. *eLife* 10: e70058, 2021. doi:10.7554/eLife.70058.
84. **Beauparlant J**, **van den Brand R**, **Barraud Q**, **Friedli L**, **Musienko P**, **Dietz V**, **Courtine G.** Undirected compensatory plasticity contributes to neuronal dysfunction after severe spinal cord injury. *Brain* 136: 3347–3361, 2013. doi:10.1093/brain/awt204.
85. **Kato M**, **Murakami S**, **Yasuda K**, **Hirayama H.** Disruption of fore- and hindlimb coordination during overground locomotion in cats with bilateral serial hemisection of the spinal cord. *Neurosci Res* 2: 27–47, 1984. doi:10.1016/0168-0102(84)90003-8.
86. **Górska T**, **Bem T**, **Majczyński H.** Locomotion in cats with ventral spinal lesions: support patterns and duration of support phases during unrestrained walking. *Acta Neurobiol Exp (Wars)* 50: 191–199, 1990.
87. **Górska T**, **Chojnicka-Gittins B**, **Majczyński H**, **Zmysłowski W.** Changes in forelimb–hindlimb coordination after partial spinal lesions of different extent in the rat. *Behav Brain Res* 239: 121–138, 2013. doi:10.1016/j.bbr.2012.10.054.
88. **Bem T**, **Górska T**, **Majczyński H**, **Zmysłowski W.** Different patterns of fore-hindlimb coordination during overground locomotion in cats with ventral and lateral spinal lesions. *Exp Brain Res* 104: 70–80, 1995. doi:10.1007/BF00229856.
89. **Alluin O**, **Karimi-Abdolrezaee S**, **Delivet-Mongrain H**, **Leblond H**, **Fehlings MG**, **Rossignol S.** Kinematic study of locomotor recovery after spinal cord clip compression injury in rats. *J Neurotrauma* 28: 1963–1981, 2011. doi:10.1089/neu.2011.1840.
90. **Arshavsky YI**, **Orlovsky GN**, **Pavlova GA**, **Popova LB.** Activity of C3-C4 propriospinal neurons during fictitious forelimb locomotion in the cat. *Brain Res* 363: 354–357, 1986. doi:10.1016/0006-8993(86)91022-X.
91. **Juvin L**, **Gal JP**, **Simmers J**, **Morin D.** Cervicolumbar coordination in mammalian quadrupedal locomotion: role of spinal thoracic circuitry and limb sensory inputs. *J Neurosci* 32: 953–965, 2012. doi:10.1523/JNEUROSCI.4640-11.2012.
92. **Juvin L**, **Simmers J**, **Morin D.** Propriospinal circuitry underlying interlimb coordination in mammalian quadrupedal locomotion. *J Neurosci* 25: 6025–6035, 2005. doi:10.1523/JNEUROSCI.0696-05.2005.
93. **Thibaudier Y**, **Hurteau MF**, **Telonio A**, **Frigon A.** Coordination between the fore- and hindlimbs is bidirectional, asymmetrically organized, and flexible during quadrupedal locomotion in the intact adult cat. *Neuroscience* 240: 13–26, 2013. doi:10.1016/j.neuroscience.2013.02.028.
94. **Cartmill M**, **Lemelin P**, **Schmitt D.** Support polygons and symmetrical gaits in mammals. *Zool J Linn Soc* 136: 401–420, 2002. doi:10.1046/j.1096-3642.2002.00038.x.